Genomic plasticity drives olfactory adaptation in a pest fly

Qi Xue[1], Hany K. M. Dweck[1, *]

[1]Department of Entomology, The Connecticut Agricultural Experiment Station, New Haven, CT 06511, USA

*Corresponding author: hany.dweck@ct.gov

SUMMARY

Preference shifts in insects are often driven by changes in the olfactory system, yet the underlying mechanisms remain unclear. The worldwide pest *Drosophila suzukii*, which oviposits in ripe rather than overripe fruits, provides a powerful model to study these mechanisms and their behavioral consequences. Here, we show that this shift is linked to functional remodeling in four olfactory receptor neurons: ab2B, ab3A, ab4B, and ab10A. While ab3A and ab10A exhibit tuning changes shared with the non-pest relative *D. biarmipes*, ab2B and ab4B display species-specific adaptations in *D. suzukii*. These changes result not only from receptor sequence divergence but also from novel innovations: receptor co-expression in ab3A and partitioned expression of Or67a paralogs in ab2B and ab10A. Together, these findings show how genomic plasticity in chemosensory gene families enables rapid sensory adaptation and niche transition.

INTRODUCTION

The olfactory system mediates the interactions between insects and their environment. It guides critical behaviors such as foraging, mate choice, and oviposition [1-4]. These behaviors are tightly linked to survival and reproductive success. This makes the olfactory system a key target of natural selection. The olfactory system, as a result, evolves rapidly in response to ecological shifts, particularly those involving changes in habitat, food resources, or reproductive sites [5-7]. However, the molecular mechanisms underlying olfactory adaptations remain poorly understood. While numerous studies have documented the remarkable variation in the copy number of chemosensory receptor genes, driven by gene gains and losses, across insect taxa[8-12], fewer have connected this genomic diversity to functional differences at the receptor and neuronal levels, or to shifts in behavior [6].

The worldwide fruit pest *D. suzukii* presents a powerful model to explore these evolutionary links. Unlike most *Drosophila* species, which are adapted to oviposit in fermenting fruit of no value, *D. suzukii* has evolved a distinct ecological niche [13,14]. It targets intact, ripening fruit for oviposition, causing significant agricultural losses[15]. This shift allows the species to exploit a previously underutilized resource, but it also poses new sensory and behavioral challenges. Navigating this niche requires the ability to detect and respond to a different set of volatile cues than those used by species that specialize on rotting substrates. Consequently, *D. suzukii*'s unique host preference is likely underpinned by extensive modifications to its olfactory system. Several molecular mechanisms are known to drive such adaptations, including amino acid substitutions that alter receptor tuning properties, changes in gene expression levels that modify receptor neuron sensitivity, and structural changes in the genome that increase or decrease receptor copy number through duplication, neofunctionalization, or pseudogenization [5,6,16-20].

Comparative genomic and transcriptomic analyses have revealed that *D. suzukii*'s odorant receptor (Or) repertoire exhibits distinctive evolutionary signatures [21-24]. Two gene expansions, *Or23a* and *Or67a*, set this species apart from its close relatives *D. biarmipes* and *D. melanogaster*. In *D. suzukii*, *Or23a* is present in four intact copies (*Or23a1*, *Or23a2*, *Or23a3*, and *Or23a4*), while *Or67a* is represented by four functional paralogs (*Or67a1*, *Or67a2*, *Or67a3*, and *Or67a4*) and one pseudogene (*Or67a5*). Interestingly, only the *Or67a* expansion is retained in *D. biarmipes* [22], suggesting that the expansion of *Or23a* occurred more recently in the *D. suzukii* lineage. In *D. melanogaster*, *Or23a* is expressed in the B neuron of antennal intermediate 2 (ai2) sensilla, but extensive functional screening has not identified strong ligands, leaving its role unresolved [25].

Or67a, by contrast, is better functionally characterized. In *D. melanogaster*, *Or67a* is expressed in the A neuron of ab10 sensilla, where it mediates strong responses to aromatic esters such as benzyl butyrate, benzyl acetate, and phenethyl propionate [25-27]. In *D. suzukii*, two copies of *Or67a* (*Or67a3* and *Or67a4*) exhibit

138 signatures of positive selection [22], suggesting adaptive evolution potentially linked to the
139 detection of odorants associated with ripening fruit.
140
141 Concurrently, *D. suzukii* has lost several ancestral Or genes, including *Or74a*,
142 *Or85a*, and *Or98b* [22,23]. These losses could represent either relaxed selection for
143 receptors tuned to volatiles no longer relevant in the new ecological context, or
144 functional trade-offs associated with receptor repertoire remodeling.
145
146 Despite these striking genomic changes, the extent to which receptor gains and
147 losses have reshaped the peripheral olfactory architecture, altering neuron identities,
148 response properties, and overall coding capacity, remains largely unexplored.
149
150 Here, through a combination of electrophysiological recordings and comparative
151 analyses, we identified olfactory receptor neurons whose response profiles differ
152 markedly between *Drosophila suzukii* and its close relatives, *D. melanogaster* and *D.*
153 *biarmipes*. Using molecular genetics, CRISPR/Cas9 gene editing, AlphaFold, and
154 molecular docking, we elucidated the molecular mechanisms underlying these neuronal
155 differences. Moreover, our work revealed that both gene losses and gains have shaped
156 the olfactory repertoire of *D. suzukii*, driving its sensory adaptation and facilitating its
157 ecological niche transition from fermenting to ripening fruits. These findings highlight
158 how molecular changes at the receptor level translate into behavioral shifts that
159 underpin the evolutionary success and pest status of *D. suzukii*.
160
161 **RESULTS**
162 **Neurons whose responses differ between *D. suzukii* and *D. melanogaster***
163 To identify neurons that differ in their responses between *D. suzukii* and *D.*
164 *melanogaster*, we compared odorant-evoked responses of olfactory receptor neurons
165 (ORNs) in the antennal basiconic, intermediate, and trichoid sensilla of both species
166 using single sensillum recordings (SSR). Modifications in the tuning of these neurons
167 could result from gene births and deaths accompanying *D. suzukii*'s transition to ripe
168 fruit[28] and may underlie its novel specialization. This analysis complements our prior
169 work on maxillary palp basiconic and antennal coeloconic sensilla in *D. suzukii* [29,30] and
170 together provides a comprehensive functional atlas of ORN responses across all
171 sensillum types.
172
173 For this analysis, we used a panel of 113 ecologically relevant odorants, each
174 tested at a 10^{-2} dilution, including acids, esters, alcohols, aldehydes, ketones, lactones,
175 and terpenes (Figure S1). This analysis generated a dataset of 3,503 odorant–ORN
176 combinations in each species (Figure S1; Extended Data Files S1 and S2) (n = 3–6 per
177 combination in *D. suzukii* and n = 3 per combination in *D. melanogaster*) and revealed
178 that the odorant response profiles of most ORNs are qualitatively similar between the
179 two species(Figure S1). However, a subset of four ORNs displayed notable shifts in
180 odorant tuning (Figure 1A). These ORNs are ab2B, ab3A, ab4B, and ab10A.
181
182 To validate and further dissect these interspecific differences, we performed a
183 second round of SSR using an odorant panel that included the most potent ligands

184 identified in our initial screen, together with ligands previously reported for the
185 corresponding ORNs[31,32]. All odorants were tested at a 10^{-4} dilution to approximate
186 naturalistic concentrations encountered by flies in the wild[33].
187
188 To differentiate between *D. suzukii*-specific changes and more broadly shared
189 evolutionary trends, we included *D. biarmipes* in our analysis. This species is the
190 closest extant relative of *D. suzukii* [34,35] and has no distinct preference for either
191 overripe or ripe fruit [13,14,21].
192
193 To assess the robustness of these shifts within *D. suzukii*, we included two
194 geographically distinct populations: the WT3 strain from California (*Dsuz*-WT3), which
195 served as the reference genome strain [34], and an independent strain collected in North
196 Carolina (*Dsuz*-NC).
197
198 **Shared and species-specific shifts in *D. suzukii***
199 In ab3A neurons, we observed two kinds of changes, one of which is shared by *D.*
200 *suzukii* and *D. biarmipes*. These included markedly reduced responses to volatiles that
201 strongly activate this neuronal type in *D. melanogaster* (Figure 1B, D, E), including ethyl
202 hexanoate, which is a fermentation product[31], and increased responses to an alternative
203 set of esters, including isoamyl acetate and butyl acetate (Figure 1D), which are
204 produced during fruit ripening[31].
205
206 The second kind of change is unique to *D. suzukii*. These included significantly
207 stronger responses to isobutyl acetate, ethyl butyrate, and ethyl isovalerate compared
208 to *D. biarmipes* and *D. melanogaster* (Figure 1D, F), as well as robust, dose-dependent
209 responses to β-cyclocitral (Figure 1C, D, G), a volatile isoprenoid emitted by green
210 foliage, including strawberry leaves[31]. By contrast, over a range of dilutions, this
211 compound elicited little or no activity in the ab3A neurons of *D. biarmipes* and *D.*
212 *melanogaster* (Figure 1C, D, G).
213
214 We also found intraspecific variation in responses to β-cyclocitral across *D.*
215 *suzukii* strains. All ab3A neurons in the WT3 strain (California origin) responded robustly
216 to β-cyclocitral, whereas responses in the North Carolina strain were more
217 heterogeneous: some ab3A neurons responded strongly while others showed little or no
218 response (Figure 1D).
219
220 In ab10A neurons, both *D. suzukii* and *D. biarmipes* exhibited reduced sensitivity
221 to benzyl butyrate and benzyl acetate compared to *D. melanogaster* (Figure 1H, I) and
222 enhanced responses to geranyl acetate, β-citronellol, isoamyl butyrate, 1-octen-3-ol,
223 ethyl-3-hydroxyhexanoate, and diethyl succinate (Figure 1H, J, K).
224
225 In ab2B neurons, both *D. melanogaster* and *D. biarmipes* exhibited strong to
226 ethyl 3-hydroxybutyrate, a compound closely associated with fermentation[36,37], whereas
227 all three *D. suzukii* strains displayed strongly reduced sensitivity (Figure 2A, C, D). By
228 contrast, ab2B neurons in *D. suzukii* responded robustly to a distinct set of esters,
229 including isoamyl acetate, butyl acetate, pentyl acetate, benzyl acetate, and isoamyl

230 butyrate (Figure 2B, C, E, F). These esters are formed as part of the fruit ripening
231 process[31,36,37].
232
233 In ab4B neurons, all three species responded to veratrole, whereas all three *D.*
234 *suzukii* strains additionally responded to ethyl salicylate, methyl salicylate, methyl
235 benzoate, acetophenone, and 4-ethylguaiacol (Figure 2G–J).
236
237 Together, these findings reveal a mosaic of shared and species-specific olfactory
238 changes in *D. suzukii*. The shifts in ab3A and ab10A, shared with *D. biarmipes*, likely
239 reflect phylogenetic divergence, whereas the unique sensitivity of ab3A neurons to β-
240 cyclocitral and species-specific tuning in ab2B and ab4B neurons point to derived
241 adaptations supporting *D. suzukii*'s specialization on ripe fruit.
242
243 ***D. suzukii* ab3A neurons co-express two odorant receptors, one of which is**
244 **specifically tuned to β-cyclocitral**
245 We next focused on ab3A neurons, which display a robust response to the strawberry
246 leaf volatile β-cyclocitral. We hypothesized that this neuronal type in *D. suzukii* co-
247 expresses two receptors, one of which is specifically tuned to β-cyclocitral. This
248 hypothesis was based on three observations: (1) only *D. suzukii* ab3A neurons respond
249 robustly to β-cyclocitral, despite both *D. suzukii* and *D. biarmipes* having a single
250 functional gene (referred to as the *Or22a*-like receptor) at the locus that determines ab3A
251 responses in drosophilids, with 91% sequence identity between the two species; (2) the
252 North Carolina strain of *D. suzukii* harbors two ab3A populations, one responsive to β-
253 cyclocitral and one not; and (3) the chemical structure of β-cyclocitral, a cyclic isoprenoid
254 aldehyde, differs markedly from the long- and short-chain esters that typically activate
255 ab3A neurons in *D. suzukii* and other *Drosophila* species.
256
257 To test this hypothesis, we first expressed the *D. suzukii Or22a* (*DsuzOr22a*) in
258 the *D. melanogaster* ab3A "empty neuron" system [38], where the endogenous
259 *Or22a*/*Or22b* locus is deleted and replaced by *Gal4* (Figure 3A). Ectopic expression of
260 *DsuzOr22a* restored responses to a suite of esters that matched the tuning profile of
261 native *D. suzukii* ab3A neurons (Figure 3B, D). However, these neurons did not confer
262 responses to β-cyclocitral (Figure 3C, D), indicating that *DsuzOr22a* is not sufficient for
263 β-cyclocitral detection and that a second co-expressed receptor is required.
264
265 We next used CRISPR/Cas9-mediated mutagenesis to generate loss-of-function
266 alleles of *DsuzOr22a*. Two independent alleles were recovered: *DsuzOr22a*^{1}, carrying a
267 25-nt deletion, and *DsuzOr22a*^{2}, carrying a 4-nt deletion. Both mutations are predicted to
268 produce truncated, non-functional proteins of 106 amino acids (Figure 3E). To control for
269 potential background effects, we also generated heteroallelic *DsuzOr22a* mutant
270 combinations using these homozygous lines.
271
272 Compared to Wild-type, *DsuzOr22a*$^{1/+}$, and *DsuzOr22a*$^{2/+}$ flies, ab3A neurons in
273 *DsuzOr22a*^{1}*, DsuzOr22a*^{2}*, and DsuzOr22a*$^{1/}$*Or22a*^{2} mutant flies exhibited drastically
274 reduced responses to all tested esters (Figure 3F, H), demonstrating that *DsuzOr22a* is
275 required for ester sensitivity. However, responses to β-cyclocitral were intact in all

mutants, confirming that a second receptor mediates detection of this compound (Figure 3G, H).

To determine whether the β-cyclocitral receptor belongs to the odorant receptor (OR) or ionotropic receptor (IR) family, we measured responses from large basiconic sensilla in *D. suzukii Orco* mutant flies. Because *Orco* is an obligate co-receptor for all functional ORs but not IRs, the presence or absence of β-cyclocitral responses in this background would distinguish the receptor class.

We found that β-cyclocitral did not elicit any response in any of the 117 individual sensilla examined in *DsuzOrco* mutant flies, indicating that β-cyclocitral detection depends on *Orco* and thus is mediated by an OR rather than an IR (Figure S2).

Together, these results demonstrate that *D. suzukii* ab3A neurons co-express two odorant receptors (Figure 3I): *Or22a*, which has shifted its tuning toward several ripening fruit esters such as isobutyl acetate, butyl acetate, and isoamyl acetate, and a second, as-yet-unidentified receptor that is specifically tuned to β-cyclocitral.

A Single Amino Acid Substitution Alters Ligand Specificity of *Or22a* in *D. suzukii*

We next investigated the molecular basis of the tuning shift of *DsuzOr22a*. To do this, we aligned the *Or22a* amino acid sequences from *D. melanogaster*, *D. suzukii*, and *D. biarmipes* using Clustal Omega and visualized the alignment with MView (Figure 4A). This analysis revealed 97 amino acid substitutions shared between *D. suzukii* and *D. biarmipes* relative to *D. melanogaster*, including a substitution at position 201 (aspartic acid [D] to alanine [A]). In *D. melanogaster* strains, the residue at this position is predicted to lie within the odorant-binding pocket[39], which is proposed to form within the extracellular leaflet of the plasma membrane between helices TM1–TM6[40]. Previous work showed variation at this site, together with changes at residue 92, alters ligand-binding specificity and contributes to phenotypic variation in ab3A responses among natural populations of *D. melanogaster*[40]. Since residue 92 is conserved across all three species, the substitution at position 201 likely plays a major role in the tuning shift of *DsuzOr22a*.

To determine the functional impact of this substitution, we used AlphaFold2 to model the wild-type DsuzOr22a (D201A) and an *in silico* variant with the A201D substitution. We then performed molecular docking with isobutyl acetate, a key ligand for *DsuzOr22a*. The predicted models revealed that the A201D substitution induces a pronounced reorganization of the binding pocket architecture, producing a conformation distinct from that of the wild-type receptor (Figure 4B). This suggests that D201A significantly alters receptor–ligand interactions and contribute to the tuning shift of *DsuzOr22a*.

We then tested this prediction by generating a site-directed mutant of *DsuzOr22a* (A201D) and expressing it in the *D. melanogaster* ab3A “empty neuron” system. This substitution did not increase the response of *DsuzOr22a* to any of the compounds that strongly activate *D. melanogaster* ab3A (Figure 4C). By contrast, it reduced responses to all tested odorants (Figure 4C, D). Interestingly, responses of the A201D variant to

isobutyl acetate across a range of dilutions more closely resembled that of *D. melanogaster* ab3A than of *D. suzukii* ab3A or wild-type *DsuzOr22a* (Figure 4D), indicating a partial reversion toward the ancestral tuning state. These results support a critical role for residue 201 in reshaping *Or22a* ligand specificity in *D. suzukii*, particularly for fruit-ripening esters.

Functional Analysis of *Or23a* and *Or67a* Paralogs in *D. suzukii*

Having demonstrated that the response to β-cyclocitral in *D. suzukii* ab3A depends on an odorant receptor other than *Or22a* and deciphered the molecular basis of the *DszuOr22a* tuning shift, we next investigated the contributions of the expanded *Or23a* (four paralogs) and *Or67a* (five paralogs) receptor subfamilies to β-cyclocitral sensitivity in ab3A neurons, as well as to tuning shifts in ab10A and ab2B neurons. To do this, we expressed each paralog individually in the *D. melanogaster* ab3A "empty neuron" system and measured odor-evoked responses across a broad panel of compounds.

We found that all *Or23a* paralogs showed little (<30 spikes/s) or no response to any of the tested odorants (Extended Data File S3), indicating that their key ligands remain unidentified. Similarly, *Or67a5* did not respond to any odorant, consistent with its annotation as a pseudogene due to a premature stop codon (TAA) at nucleotide position 174 (Extended Data File S4).

By contrast, *Or67a1*, *Or67a2*, *Or67a3*, and *Or67a4* each exhibited robust and specific responses to multiple odorants (Figures 5). However, none of these receptors responded to β-cyclocitral with the same magnitude or sensitivity as the native ab3A neuron, indicating that the receptor mediating this response remains unidentified.

Co-expression of *Or67a1* and *Or67a2* Produces a Response Profile Closely Matching the Native ab10A Odor Response in *D. suzukii*

Or67a1 and *Or67a2* responded to an overlapping set of odorants, but differed in response magnitude for several compounds, including geranyl acetate, α-phellandrene, and β-citronellol (Figure 5A). The odorant response profile of *Or67a2* more closely resembled that of the native *D. suzukii* ab10A neurons than did *Or67a1* (Figure 5A), with a mean Euclidean distance of 116 ± 0.8 (SE) compared to 122 ± 1 for *Or67a1*.

To determine whether co-expression of both receptors is required to fully replicate the ab10A response profile, we expressed *Or67a1* and *Or67a2* together in the *D. melanogaster* ab3A "empty neuron" system. This co-expression produced responses that closely matched the ab10A response profile (Figure 5A), with a smaller Euclidean distance (107 ± 2.5) than either receptor alone. The simple interpretation of these results is that *Or67a1* and *Or67a2* are co-expressed in the *D. suzukii* ab10A neurons and that their combined activity produces the characteristic tuning of this neuronal type.

***Or67a4* is expressed in the ab2B neurons of *D. suzukii* and mediates their odorant responses**

Or67a3 and *Or67a4*, on the other hand, displayed odorant response profiles that diverged markedly from that of ab10A neurons (Figure 5B). Surprisingly, the response profile of

368 each of *Or67a3* and *Or67a4* closely resembled that of the native *D. suzukii* ab2B neurons
369 (Figure 5B), with Or67a4 showing a smaller mean Euclidean distance (180 ± 2.5)
370 compared to Or67a3 (319 ± 2.7). However, co-expression of *Or67a3* and *Or67a4* in the
371 *D. melanogaster* ab3A 'empty neuron' system produced a response profile more similar
372 to *Or67a3* (192 ± 1.4 SE, mean Euclidean distance) than to either the native *D. suzukii*
373 ab2B (229 ± 2.5) or *Or67a4* alone (218 ± 1.1) (Figure 5B). The simple interpretation of
374 these results is that both *Or67a3* and *Or67a4* are expressed in ab2B neurons, since no
375 other ORNs besides ab2B produce responses resembling those of *Or67a3*, with *Or67a4*
376 dominating the overall odorant response profile in the native ab2B, likely due to higher
377 expression levels. Consistent with this, *Or67a4* expression increases significantly after
378 mating, while Or67a3 expression remains unchanged[41].
379
380 We further confirmed and extended these findings by generating two independent
381 loss-of-function alleles of *DsuzOr67a4* using CRISPR/Cas9: one with two deletions (22
382 bp and 47 bp; *DsuzOr67a4*^{1}) (*DsuzOr67a4*^{2}) and the other with a 22-bp deletion (Figure
383 S3). From these homozygous mutants, we also established two heterozygous lines.
384
385 While wild-type and heterozygous lines responded indistinguishably, ab2B
386 neurons in the two *DsuzOr67a4* mutant alleles exhibited markedly reduced responses to
387 all tested odorants (Figure 5C). This indicates that *Or67a4* is expressed in *D. suzukii* ab2B
388 neurons and is essential for their odorant responses. Alternatively, because *Or67a4* lies
389 only 380 bp upstream of *Or67a3* and the two genes appear to undergo transcriptional
390 readthrough (Figure S3C), its deletion could disrupt shared regulatory elements or
391 chromatin structure, thereby altering *Or67a3* transcription. The phenotype may thus
392 reflect both *Or67a4* loss and secondary effects on O*r67a3*.
393
394 Together, these findings reveal a clear functional and spatial partitioning among
395 the *Or67a* paralogs in *D. suzukii*. *Or67a1* and *Or67a2* are co-expressed in ab10A
396 neurons, while *Or67a4* and *Or67a3* are expressed in a separate neuronal type, ab2B.
397 This partitioning of expression suggests that gene duplication in the *Or67a* lineage has
398 facilitated subfunctionalization across distinct olfactory neuron types, enabling *D. suzukii*
399 to broaden its olfactory repertoire and fine-tune its detection of ecologically relevant
400 odorants.
401
402 **Species-Specific Partitioned Expression of Or67a Paralogs in Drosophila suzukii**
403 To determine whether the evolutionary expansion of the *Or67a* subfamily in *D. suzukii* is
404 associated with species-specific adaptations, we first inferred a maximum likelihood
405 protein tree for the five *D. suzukii* paralogs (*Or67a1*, *Or67a2*, *Or67a3*, *Or67a4*, and
406 *Or67a5*), the four *D. biarmipes* paralogs (*Or67a1*, *Or67a2*, *Or67a3*, and *Or67a5*), and *D.*
407 *melanogaster Or67a*. We confirmed the absence of *Or67a4* in *D. biarmipes* through
408 genome inspection and BLAST searches of the NCBI database using the *D. suzukii*
409 *Or67a4* sequence.
410
411 This analysis revealed that the *Or67a* subfamily in *D. suzukii* is shaped by both
412 conservation and lineage-specific innovation. *D. suzukii* and *D. biarmipes Or67a5*
413 clustered with *D. melanogaster Or67a* with strong support (96 bootstrap) (Figure 6A),

414 identifying it as the conserved ancestral ortholog that became pseudogenized in *D.*
415 *suzukii*. *D. suzukii Or67a3* and *D. biarmipes Or67a3* clustered with *D. suzukii Or67a4* with
416 full support (100 bootstrap) (Figure 6A), indicating that *Or67a4* originated through a
417 lineage-specific duplication and divergence event in *D. suzukii*. By contrast, *D. suzukii*
418 *Or67a1* and *Or67a2* each clustered with their *D. biarmipes* orthologs (100 bootstrap)
419 (Figure 6A).
420
421 We next characterized the responses of *D. biarmipes Or67a* paralogs. Specifically,
422 we asked whether the four intact *D. biarmipes* paralogs map onto the same neuronal
423 classes (ab2B and ab10A) as in *D. suzukii* and whether their odor response profiles reflect
424 conserved tuning or reveal species-specific divergence.
425
426 This analysis revealed that none of the *D. biarmipes Or67a* paralogs produced
427 responses resembling those of ab2B neurons (Figure 6B; Extended Data File S5),
428 indicating that the partitioned expression of *Or67a* paralogs between ab10A and ab2B is
429 unique to *D. suzukii*.
430
431 *D. biarmipes Or67a1* and *Or67a2* responses closely resemble those of their *D.*
432 *suzukii* orthologs (Figure 6B, C), reflecting both functional conservation and their close
433 evolutionary relationships in the protein-based phylogenetic tree. However, *D. biarmipes*
434 *Or67a2* responded to fewer compounds than its *D. suzukii* counterpart. These receptors
435 appear to be expressed in ab10A neurons, as their responses closely match those of
436 ab10A than of ab2B (Figure 6B).
437
438 *D. biarmipes Or67a5* showed strong responses to ethyl benzoate and methyl
439 benzoate (Figure 6B), two of the best activators of the ancestral *Or67a* in *D.*
440 *melanogaster*[27]. This functional conservation aligns with its clustering alongside *D.*
441 *melanogaster Or67a* in the protein-based phylogenetic tree (Figure 6A). In *D. biarmipes*,
442 ab10A neurons likely express this receptor, as these compounds are their strongest
443 activators (Figure 6B). By contrast, the Or67a5 ortholog in *D. suzukii* is pseudogenized,
444 and its ab10A neurons showed little or no response to these compounds (Figure 5A).
445
446 Most *Or67a3* responses are conserved between *D. biarmipes* and *D. suzukii*
447 (Figure 6B, C), implying that this tuning profile evolved prior to the ecological shift of *D.*
448 *suzukii* to exploit ripe fruit. *In D. suzukii*, *Or67a3* responses closely resemble those of
449 ab2B (Figure 5B), whereas in *D. biarmipes*, *Or67a3* responses do not (Figure 6B),
450 suggesting that this receptor likely remains expressed in ab10A neurons and that its
451 functional contribution may be partially masked by co-expressed receptors within the
452 same neuronal type. This is consistent with observations in taste neurons, where co-
453 expression of multiple gustatory receptors can obscure individual contributions, and
454 deletion of specific receptors often reveals novel responses[42].
455
456 Altogether, these results support a model for the partitioning of Or67a paralog
457 expression between two distinct neuronal types, ab10A and ab2B, in *D. suzukii* (Figure
458 6D). This scenario likely began with the ancestral expansion of *Or67a* into four paralogs
459 (*Or67a1*, *Or67a2*, *Or67a3*, and *Or67a5*) in *D. biarmipes*, all of which were expressed in

the ancestral ab10A neurons, with *Or67a1*, *Or67a2,* and *Or67a5* dominating the odorant response profile of this neuron type. In *D. suzukii*, the ecological shift toward exploiting ripe fruit coincided with the pseudogenization of *Or67a5* and the loss of *Or85a* expression in ab2B neurons. This loss was compensated by the emergence of *Or67a4*, which relocated to only 380 bp upstream of *Or67a3*. This genomic rearrangement likely altered regulatory elements, allowing both *Or67a3* and *Or67a4* to be expressed in ab2B neurons, thereby replacing *Or85a* and shaping the ab2B response profile of *D. suzukii* for fruit-ripening esters.

DISCUSSION

Our results reveal that the evolutionary shift in preference from overripe to ripe fruit in *Drosophila suzukii,* a worldwide berry fly pest*,* is mirrored by functional changes in a limited subset of ORNs. Specifically, four ORNs (ab2B, ab3A, ab4B, and ab10A) exhibit altered odorant tuning in *D. suzukii* relative to *D. melanogaster*. Of these, ab3A and ab10A exhibit shared tuning shifts in *D. suzukii* and its non-pest sibling species *D. biarmipes*. These shared shifts likely reflect ancestral adaptations predating the transition to ripe fruit use. By contrast, ab2B and ab4B show unique tuning profiles in *D. suzukii*.

Importantly, these modifications are not solely the result of receptor sequence evolution but are also mediated by innovative mechanisms, including the co-expression of two distinct odorant receptors in a single ORN (as observed in ab3A) and the partitioned expression of gene duplicates across different ORNs (as seen with the *Or67a* paralogs in ab2B and ab10A). These strategies provide a flexible framework for expanding olfactory function without requiring the evolution of entirely new neuronal types, facilitating rapid and efficient sensory adaptation during ecological transitions.

Receptor Co-expression Enables Novel Odor Tuning in ab3A of *D. suzukii*

The ab3A neurons of *D. suzukii* illustrate two distinct molecular innovations that align with its shift to ripe fruit. First, these neurons have lost responses to key fermentation volatiles that strongly activate ab3A in *D. melanogaster*. Instead, they have gained increased sensitivity to a new set of ripening-associated short-chain esters. Second, ab3A neurons in *D. suzukii* have acquired strong sensitivity to β-cyclocitral, a volatile isoprenoid commonly found in green plant tissues such as strawberry leaves[31]. This represents a major functional innovation, as neither *D. melanogaster* nor *D. biarmipes* ab3A neurons respond to this compound. Thus, detection of β-cyclocitral likely serves as a vegetative cue that signals the presence of a host plant bearing fruit, providing *D. suzukii* with a sensory advantage in locating oviposition sites while the fruit is still attached to the plant.

The capacity for functional plasticity in ab3A neurons is a recurring theme in *Drosophila* evolution. This neuronal type has repeatedly shifted its odorant tuning across species and even among populations, often in response to divergent ecological pressures[39,43-47]. These shifts are frequently mediated by amino acid changes in the *Or22* locus, which encodes the primary odorant receptor(s) in ab3A[20,45,47]. In the noni-specialist *D. sechellia*, for example, *Or22a* has acquired substitutions that enhance its sensitivity to methyl esters, which are abundant in noni fruit[45]. Genetic approaches have demonstrated

that these sequence changes are sufficient to alter the ab3A sensitivity and that this receptor is important for mediating long-range attraction to noni[45].

Similarly, in *D. suzukii*, we identified multiple amino acid substitutions in *Or22a*, including two at known functional hotspots, I45A and D201A, previously implicated in tuning modulation in other *Drosophila* species[20,45]. Our structural modeling and molecular docking analyses indicate that the D201A substitution plays a key role in the tuning shift of *Or22a* in *D. suzukii*. This substitution reorganizes the architecture of the ligand-binding pocket, likely altering the shape and electrostatic environment of the odorant interface. Furthermore, functional assays using a site-directed A201D mutant revealed markedly reduced responses to odorants, with its responses to isobutyl acetate across dilutions more closely resembling those of *D. melanogaster* ab3A than *D. suzukii* ab3A or wild-type *DsuzOr22a*, indicating partial reversion to the ancestral tuning state. However, similar tuning shifts and a substitution at position 201 were also observed in *D. biarmipes*, suggesting that *Or22a* diversification occurred prior to the shift to ripe fruit and may have evolved under different selective pressures.

Despite the functional impact of *Or22a* sequence evolution, it alone cannot account for the novel β-cyclocitral sensitivity. This response is absent in both *D. melanogaster* and *D. biarmipes*, indicating that the gain of β-cyclocitral sensitivity is a derived feature unique to *D. suzukii*. Our genetic and functional analyses revealed that β-cyclocitral sensitivity is mediated by a second odorant receptor co-expressed with *Or22a* in ab3A neurons. The response to β-cyclocitral was eliminated in *Orco* mutant flies confirming that the receptor that mediates this response belongs to the OR family rather than the ionotropic or gustatory receptor families. Recruitment of a second receptor likely reflects the chemical dissimilarity of β-cyclocitral from typical *Or22a* ligands and represents a strategic expansion of the odorant space encoded by a single ORN. This co-expression may also enable more refined odorant coding: combined input from both receptors indicates the presence of a high-quality oviposition site, while activation of *Or22a* alone signals suboptimal substrates. Such combinatorial coding could sharpen host selection and oviposition decisions.

Or67a Gene Family Expansion and Deployment Across Neurons

The ab10A and ab2B neurons in *D. suzukii* have also undergone substantial functional and molecular remodeling. In *D. melanogaster*, ab10A neurons express a single receptor, *Or67a*, tuned to a broad range of compounds[25,26], whereas ab2B neurons express *Or85a*, which responds to esters and alcohols typically associated with microbial fruit degradation[25-27,36].

The response profiles of these two neuronal types have shifted markedly during *Drosophila* evolution[32,48,49]. Changes in ab10A are likely driven by *Or67a* gene expansion; for example, *D. simulans* carries three *Or67a* paralogs, all expressed in ab10A and contributing to its novel response profile[16]. By contrast, the mechanisms underlying ab2B tuning shifts remain less well understood. In several species, changes in ab2B odorant response profiles are associated with the loss of *Or85a*[48,49], but the receptors that replace it remain unidentified.

552
553 In *D. suzukii*, *Or85a* is not detected in the genome[22,23], while *Or67a* has
554 expanded into five paralogs: four intact paralogs (*Or67a1* through *Or67a4*) and one
555 pseudogene, *Or67a5*, which contains a premature stop codon[22,23]. Our functional
556 characterization of these paralogs revealed a clear partitioning of activity. *Or67a1* and
557 *Or67a2* are likely co-expressed in ab10A neurons, and their co-expression produced a
558 response profile that is more similar to that of ab10A than either receptor alone. By
559 contrast, Or67a4 and Or67a3 exhibited responses that are similar to those of ab2B
560 neurons, and deletion of *Or67a4* severely reduced ab2B responses to odorants,
561 providing direct evidence that this receptor underlies the novel tuning of ab2B neurons
562 in *D. suzukii*.
563
564 *D. biarmipes* has also expanded *Or67a* into four functional paralogs (*Or67a1*,
565 *Or67a2*, *Or67a3*, and *Or67a5*). Genome inspection and BLAST searches confirmed the
566 absence of *Or67a4* in this species, indicating that this paralog is unique to *D. suzukii*. *In*
567 *D. suzukii*, *Or67a4* relocated to 380 bp upstream of *Or67a3*, likely altering regulatory
568 elements to enable co-expression of both receptors in ab2B neurons.
569
570 The tuning shift in *D. biarmipes* ab10A neurons is likely driven by co-expression
571 of all *Or67a* paralogs, similar to *D. simulans*[16]. This conclusion is supported by several
572 observations: First, none of the *D. biarmipes Or67a* paralogs produce responses
573 resembling those of ab2B neurons, and ab2B neurons retain a *D. melanogaster*-like
574 odorant response profile, consistent with the presence of *Or85a* in its genome. Second,
575 *D. biarmipes Or67a1* and *Or67a2* responses closely resemble those of their *D. suzukii*
576 orthologs. These receptors are likely expressed in ab10A neurons, as in *D. suzukii*,
577 given that their responses more closely match ab10A than ab2B. Third, *D. biarmipes*
578 *Or67a5* exhibits robust responses to ethyl benzoate and methyl benzoate, which are the
579 strongest activators of both the ancestral *Or67a* in *D. melanogaster*[27] and ab10A
580 neurons in *D. biarmipes*. Fourth, although most responses of *D. biarmipes Or67a3*
581 resemble those of *DsuzOr67a3*, ab2B responses in *D. biarmipes* are entirely different.
582 Some responses of *Or67a3* instead resemble those of ab10A, suggesting that its
583 activity may be masked by co-expression with other *or67a* receptors in ab10A.
584
585 These differences suggest that the recruitment of *Or67a4* and *Or67a3* into the
586 ab2B neurons is a unique feature to *D. suzukii*, likely emerging after the genomic loss of
587 *Or85a* and the gain of *Or67a4*. As such, *D. biarmipes* represents an intermediate
588 evolutionary state: while it shows early signs of olfactory adaptation in ab3A and ab10A
589 neurons, it does not exhibit β-cyclocitral sensitivity in ab3A neurons, which in *D. suzukii*
590 arises from the co-expression of a second receptor alongside *Or22a*, nor does it show
591 evidence for receptor reassignment in ab2B.
592
593 In summary, by co-expressing a second OR with *Or22a* in ab3A and partitioning
594 *Or67a* paralogs between ab10A and ab2B, *D. suzukii* expands its odorant tuning
595 without creating new neuronal classes or rewiring central circuits. This illustrates how
596 gene loss, duplication, functional divergence, and receptor redeployment can reprogram
597 olfactory function to meet the demands of novel ecological niches.

Limitations of the study

Although we elucidated that *D. suzukii* ab3A neurons express an additional receptor enabling detection of β-cyclocitral, the identity of this receptor remains unknown. Additionally, while our data indicate that *Or67a1* and *Or67a2* are co-expressed in ab10A neurons and that *Or67a4* has replaced the ancestral *Or85a* in ab2B neurons, *Or67a3* is also a strong candidate for ab2B expression, as its ectopic expression produces responses resembling those of native ab2B neurons, and no other ORN responses resemble those of Or67a3. Notably, *Or67a3* lies immediately downstream of *Or67a4*, separated by fewer than 500 base pairs, raising the possibility that our CRISPR-mediated knockout of *Or67a4* may have inadvertently affected *Or67a3* expression. Finally, the regulatory mechanisms governing the partitioned expression of *Or67a* paralogs across these distinct neurons in *D. suzukii* remain unresolved.

Methods

Drosophila stocks

Flies, 5-7 days old, were reared on corn syrup and soy four culture medium (Archon Scientifc) at 24°C and 50% relative humidity in a 12:12-h light–dark cycle. *D. melanogaster* Canton-S stock was CS-5. *D. suzukii* Connecticut (CT), North Carolina (NC), and California genome (WT3) strains were obtained from Dr. Richard S. Cowles, Dr. Maxwell J. Scott, and Dr. Joanna C. Chiu, respectively. *D. biarmipes* (14,023–0361.04) stock was obtained from the Drosophila Species Stock Center. *D. suzukii* $Orco^{3}$ mutant line was obtained from Dr. Benjamin Prud'homme. The *D. melanogaster* empty neuron system ($Or22ab^{Gal4}$) was obtained from Dr. John R. Carlson.

Odorants

Odorants of the highest available purity were obtained from Millipore Sigma, TCI America, or Thermo Scientific Chemicals and stored as recommended. A complete list of odorants is provided in Table S1. Odorants were dissolved in hexane (Millipore Sigma, Catalog #139386). Odor presentation was performed by inserting a Pasteur pipette tip into a hole in a 20 cm delivery tube, which directed a continuous airstream over the labium. The airflow through the pipette was controlled using a Stimulus Air Controller CS-55 V2 (Syntech), delivering a 0.5 s pulse. The wind speed at the position of the mounted animal, after adding the odorized stimulus to the continuous airflow, was approximately 50 cm s^{-1}. As an odor source, a cellulose filter disc (~1 cm diameter) soaked with 10 µl of diluted odorant was placed inside a disposable borosilicate glass Pasteur pipette (2 ml capacity, Fisher Scientific GSA). Odorants were presented sequentially, with at least 60 s between presentations. For dose–response analyses, odorants were delivered in increasing concentrations in logarithmic steps.

Electrophysiology

A single fly was placed in a 200-µL plastic pipette tip with its head directed towards the narrower end to allow only the antennae to protrude. The pipette tip was then securely attached to a glass microscope slide. The antenna was gently stabilized on a cover slip using a glass capillary. The slide was then placed under a light microscope (BX51WI, Olympus, Tokyo, Japan) equipped with a 50 × objective (LMPLFLN 50X, Olympus) and

644 10 × eyepieces. A reference tungsten electrode (catalog no. 716000, A-M Systems),
645 electrolytically sharpened to 1 μm tip diameter by dipping it repeatedly in a 10% KNO3
646 solution, was inserted into the eye. The recording tungsten electrode, identical to the
647 reference electrode, was inserted gently into the base of a coeloconic sensillum. Signals
648 were amplified (10 × ; Syntech Universal AC/DC Probe; http://www.syntech.nl), sampled
649 (10,667 samples s^{-1}), and filtered (100–3000 Hz with 50/60 Hz suppression) via a USB-
650 IDAC connection (Syntech) to a computer. Action potentials were extracted using
651 Syntech AutoSpike 32 software. Responses as the increase (or decrease) in the action
652 potential frequency (spikes/s) were calculated by subtracting the number of action
653 potentials during the 0.5 s preceding the odor stimulation from the number of action
654 potentials during the 0.5 s of odor stimulation. We then subtracted the response to
655 hexane from the response to the odorant, and the differences are what we reported.
656
657 **Continuous airflow**
658 A 20 cm glass tube with an inner diameter of approximately 4 mm supplied activated
659 charcoal-filtered humidified air to the labium. Air, continuous and pulsed, was generated
660 by a Stimulus Air Controller CS-55 V2 from Syntech (https://www.ockenfels-
661 syntech.com/products/stimulus-controllers/). The end of the tube was placed about 1 cm
662 from the preparation, and the continuous airflow near the mounted animal had a speed
663 of approximately 40 cm s−1.
664
665 ***Generating UAS-DsuzOr* lines**
666 Five *D. suzukii* WT3 females were collected, and whole animals were immediately
667 homogenized for RNA extraction using TRIzol reagent (Invitrogen). The extracted RNA
668 was treated with TURBO DNase (Invitrogen) to remove residual genomic DNA. 1 μg of
669 purified RNA was used for cDNA synthesis with oligo(dT) primers using SuperScript IV
670 Reverse Transcriptase (Invitrogen) for the generation of PCR template for subsequent
671 amplifications of *DsuzOr* genes. PCR reactions were conducted using Phusion High-
672 Fidelity DNA Polymerase (Thermo Scientific) under standard thermal cycling conditions
673 in a Bio-Rad thermocycler. PCR products were separated on 1.0% agarose gel, and
674 DNA fragments of the expected sizes were excised and purified according to the
675 manufacturer's instructions (Wizard SV Gel and PCR Cleanup System, Promega).
676
677 *DsuzOrs* were cloned into the pJFRC81-10XUAS-IVS-Syn21-GFP-p10 vector
678 (pJFRC81, Addgene plasmid #36432). Forward and reverse PCR primers
679 of *DsuzOrs* were designed with 20 bp overhangs complementary to the regions flanking
680 the GFP coding sequence in pJFRC81. The pJFRC81 vector was linearized by PCR
681 using primers flanking the GFP sequence, with effective removal of the GFP coding
682 region. Gibson assembly (NEB) was then used to ligate the amplified *DsuzOr* fragments
683 into the linearized vector. The resulting constructs were transformed into bacteria and
684 sequence-verified. Verified plasmids were injected into embryos of BDSC Stock #8622
685 by BestGene Inc. for PhiC31-mediated site-specific integration. Primers are provided in
686 Table S2.
687
688 **CRISPR–Cas9-mediated genome engineering**

689 Single guide RNAs (sgRNAs) targeting *DsuzOrs* were designed using the online
690 CHOPCHOP tool (https://chopchop.cbu.uib.no/). sgRNAs were synthesized through *in*
691 *vitro* transcription using the GeneArt Precision gRNA Synthesis Kit (Thermo Fisher
692 Scientific). The sgRNA was mixed with Cas9 protein (TrueCut, Invitrogen) at a final
693 concentration of 200 ng/µl and 500ng/µl, respectively, in a 10 µl reaction with 1 µl of
694 injection buffer (300 mM sodium phosphate and 1 mM potassium chloride) and an
695 additional 1 µl of 2M potassium chloride. The sgRNA/Cas9 mixture was incubated at
696 37ºC for 10 min in a thermocycler to promote ribonucleoprotein (RNP) complex
697 formation. The resulting RNP solution was passed through a Millipore Ultrafree-MC filter
698 (0.45 µM pore size) and kept on ice until ready to use.
699
700 The microinjection of RNPs into *Drosophila* embryos was performed using a
701 FemtoJet 4i microinjector (Eppendorf). Injection needles were prepared from capillary
702 tubes (World Precision Instrument, 1B100F-4) using a micropipette puller (Model P-
703 1000, Sutter Instrument). One day before microinjection, approximately 300 flies (3-5
704 days old) were transferred to an egg-laying chamber (Flystuff Cat #59-100) containing a
705 Petri dish filled with 10 ml of egg-laying substrate composed of 25g agar and 200ml
706 molasses dissolved in 500 ml of water. To diminish the older eggs retained in the
707 females' ovaries, the egg-laying Petri dish was replaced every 20 min for at least 5
708 times before injection. Only embryos laid within 20 min were used for injection, and the
709 entire injection process was completed within 1h.
710
711 G0 females that emerged from injected embryos (G0) were crossed to wild-type
712 flies to generate G1 heterozygotes. G1 individuals with potential CRISPR-induced
713 mutations were crossed again to wild-type flies to produce G2 heterozygotes. G1 flies
714 were sacrificed for genotyping to confirm the mutation types. G2 heterozygotes were
715 self-crossed to obtain homozygous mutants and establish stable mutant lines. Mutants
716 were identified using a PCR-based screening strategy. Primers for sgRNA synthesis
717 and mutant screening are listed in Table S3.
718
719 **Structural prediction and molecular docking.**
720 The 3D homotetrameric structures of *DsuzOr22a*$^{WT(D201A)}$ and *DsuzOr22a*^{A201D} were
721 generated with AlphaFold2[50]. The highest-confidence predictions (*model_0*) were
722 selected for docking. The ligand, isobutyl acetate (SDF file), was obtained from
723 PubChem (https://pubchem.ncbi.nlm.nih.gov/) and converted to mol2 format with
724 OpenBabel (v3.1.1)[51]. Structural preparation of both the ligand and receptor subunits
725 was performed in PyMol (v3.1.4), and the resulting files were converted to PDBQT
726 format with AutoDockTools (v1.5.7). Molecular docking was carried out using AutoDock
727 Vina (v1.2.7) with a cubic grid box (20 Å x 20 Å x 20 Å) centered on the transmembrane
728 domains. Receptor–ligand interactions were analyzed with the Protein-Ligand
729 Interaction Profiler (v2.4.0) and visualized in PyMol (v3.1.4).
730
731 **Maximum-likelihood phylogenetic trees**
732 To construct maximum-likelihood phylogenetic trees of the Or67a subfamily, we
733 retrieved the amino acid sequences of D. suzukii and D. biarmipes Or67a paralogs, as
734 well as D. melanogaster Or67a, from NCBI. Sequences were aligned using ClustalW in

MEGA version 11 with default parameters. We then used MEGA's "Find Best Protein Models (ML)" to select the best-fit substitution model based on the lowest Bayesian Information Criterion (BIC) score. This model was applied to generate maximum-likelihood trees with 1,000 bootstrap replicates to assess branch support.

Quantification and statistical analysis

The heatmaps were generated in PAST. Euclidean distances were calculated in R (version 4.2.3) using the 'moments' package, and other statistical tests were performed in GraphPad Prism (version 10.0.1 [316]).

Acknowledgements

This work was supported by NIH grant K01 DC020145 to H.K.M.D.

Contributions

H.K.M.D. conceived the study. H.K.M.D. and Q.X. designed the experiments. H.K.M.D. and Q.X. carried out the experiments. H.K.M.D. and Q.X. analysed the data. H.K.M.D. and Q.X. prepared the original draft of the manuscript. H.K.M.D. and Q.X. read and approved the final version of the manuscript.

Figure legends

Figure 1. Shared shifts in odor tuning of ab3A and ab10A in *D. suzukii* and *D. biarmipes*.

((A) Responses of ab2B, ab3A, ab4B, and ab10A neurons in *D. suzukii* (n = 3–6) and *D. melanogaster* (n = 3) to the indicated odorants, each tested at a 10^{-2} dilution. Error bars represent SEM. Responses to additional odorants are shown in Figure S1 and Extended Data Files S1 and S2.

(B) Example traces of the response of the ab3 sensillum type to a 10^{-4} dilution of ethyl hexanoate in *D. suzukii* (CT-strain), *D. biarmipes*, and *D. melanogaster*.

(C) Example traces of the response of the ab3 sensillum type to a 10^{-4} dilution of β-cyclocitral in *D. suzukii* (CT-strain), *D. biarmipes*, and *D. melanogaster*.

(D) Responses of ab3A neurons in three strains of *D. suzukii* (*Dsuz-CT*, *Dsuz-NC*, and *Dsuz*-WT3), *D. biarmipes*, and *D. melanogaster* to a 10^{-4} dilution of each of the indicated odorants. One-way ANOVA followed by Tukey's multiple comparison test; n = 10. Values marked with different letters are significantly different. Error bars represent SEM.

(E-G) Responses of ab3A neurons to different dilutions of ethyl hexanoate (E), isobutyl acetate (F), and β-cyclocitral (G) in *D. suzukii* (CT-strain), *D. biarmipes*, and *D. melanogaster*. One-way ANOVA followed by Tukey's multiple comparison test; n = 5 for each dilution. Values indicated with different letters are significantly different. Error bars represent SEM.

780 (H) Responses of ab10A neurons in three strains of *D. suzukii*, *D. biarmipes*, and *D.*
781 *melanogaster* to a 10^{-4} dilution of each of the indicated odorants. One-way ANOVA
782 followed by Tukey's multiple comparison test; n = 10. Values indicated with different
783 letters are significantly different. Error bars represent SEM.
784
785 (I-K) Responses of ab10A neurons to different dilutions of benzyl butyrate (I), β-
786 citronellol (J), and geranyl acetate (K) in *D. suzukii* (CT-strain), *D. biarmipes*, and *D.*
787 *melanogaster*. One-way ANOVA followed by Tukey's multiple comparison test; n = 5 for
788 each dilution. Values indicated with different letters are significantly different. Error bars
789 represent SEM.
790
791 **Figure 2. Species-specific shifts in odor tuning of ab2B and ab4B in *D. suzukii*.**
792 (A) Example traces of the response of the ab2 sensillum type to a 10^{-4} dilution of ethyl
793 3-hydroxybutyrate in *D. suzukii* (CT-strain), *D. biarmipes*, and *D. melanogaster*.
794
795 (B) Example traces of the response of the ab2 sensillum type to a 10^{-4} dilution of
796 isoamyl acetate in *D. suzukii* (CT-strain), *D. biarmipes*, and *D. melanogaster*.
797
798 (C) Responses of ab2B neurons in three strains of *D. suzukii*, *D. biarmipes*, and *D.*
799 *melanogaster* to a 10^{-4} dilution of each of the indicated odorants. One-way ANOVA
800 followed by Tukey's multiple comparison test; n = 10. Values marked with different
801 letters are significantly different. Error bars represent SEM.
802
803 (D-F) Responses of ab2B neurons to different dilutions of ethyl 3-hydroxybutyrate (D),
804 isoamyl acetate (E), and butyl acetate (F) in *D. suzukii* (CT-strain), *D. biarmipes*, and *D.*
805 *melanogaster*. One-way ANOVA followed by Tukey's multiple comparison test; n = 5 for
806 each dilution. Values indicated with different letters are significantly different. Error bars
807 represent SEM.
808
809 (G) Responses of ab4B neurons in three strains of *D. suzukii*, *D. biarmipes*, and *D.*
810 *melanogaster* to a10^{-4} dilution of the indicated odorants. One-way ANOVA followed by
811 Tukey's multiple comparison test; n = 10. Values indicated with different letters are
812 significantly different. Error bars represent SEM.
813
814 (H-J) Responses of ab4B neurons to different dilutions of ethyl salicylate (H), methyl
815 salicylate (I), and methyl benzoate (J) in *D. suzukii* (CT-strain), *D. biarmipes*, and *D.*
816 *melanogaster*. One-way ANOVA followed by Tukey's multiple comparison test; n = 5 for
817 each dilution. Values indicated with different letters are significantly different. Error bars
818 represent SEM.
819
820 **Figure 3. ab3A neurons in *D. suzukii* express two odorant receptors, one of which**
821 **is tuned to β-cyclocitral.**
822 (A) Illustration of the *D. melanogaster* empty neuron system.
823
824 (B) Example traces of the responses of *D. suzukii* ab3A neurons and *DsuzOr22a* to a
825 10^{-4} dilution of isobutyl acetate.

826
827 (C) Example traces of the responses of *D. suzukii* ab3A neurons and *DsuzOr22a* to a
828 10^{-4} dilution of β-cyclocitral.
829
830 (D) Responses of *D. suzukii* ab3A neurons and *DsuzOr22a* to eleven odorants, each
831 tested at a 10^{-4} dilution. ns = not significant; ****p<0.0001; Mann-Whitney test; n = 10.
832 Error bars represent SEM.
833
834 (E) Schematic illustrating the generation of *DsuzOr22a* mutants using CRISPR/Cas9.
835 Nucleotides in pink represent the PAM site, underlined nucleotides indicate the gRNA
836 sequence, and dashed lines denote deleted nucleotides.
837
838
839 (F) Example traces of the responses of ab3A neurons in wild-type *D. suzukii*,
840 $DsuzOr22a^{1}$, and $DsuzOr22a^{2}$ to a 10^{-4} dilution of isobutyl acetate.
841
842 (G) Example traces of the responses of ab3A neurons in wild-type *D. suzukii*,
843 $DsuzOr22a^{1}$, and $DsuzOr22a^{2}$ to a 10^{-4} dilution of β-cyclocitral.
844
845 (H) Responses of ab3A neurons in wild-type *D. suzukii*, $DsuzOr22a^{1/+}$, $DsuzOr22a^{2/+}$,
846 $DsuzOr22a^{1}$, and $DsuzOr22a^{2}$ to a panel of eleven odorants, each tested at a 10^{-4}
847 dilution. One-way ANOVA followed by Tukey's multiple comparison test; n = 10. Values
848 indicated with different letters are significantly different. Error bars represent SEM.
849
850 (I) Diagrams of ab3 sensilla in *D. melanogaster*, *D. biarmipes*, and *D. suzukii*. In *D.*
851 *melanogaster* and *D. biarmipes*, the ab3A neuronal type expresses a single odorant
852 receptor (*Or22a*), whereas in *D. suzukii* it co-expresses two receptors (*Or22a* and *Orx*).
853
854 **Figure 4. A single amino acid substitution alters the architecture of the ligand-**
855 **binding pocket of Or22a in *D. suzukii*.**
856 (A) Protein sequence alignment of Or22a orthologs of *D. melanogaster*, *D. suzukii*, and
857 *D. biarmipes*. Predicted transmembrane (TM) domains are indicated with black lines.
858 Yellow shading highlights amino acids conserved between *D. suzukii* and *D. biarmipes*
859 but differing from D. melanogaster. Cyan shading marks the amino acid at position 201
860 in all three species. PID indicates percent sequence identity.
861
862 (B) Cartoon models of $DsuzOr22a^{WT(D201A)}$ (left) and $DsuzOr22a^{(A201D)}$ (right) in lateral
863 view, showing the predicted binding sites with docked isobutyl acetate. Position 201 is
864 highlighted in cyan.
865
866 (C) Responses of wild-type *D. suzukii* ab3A neurons, $DsuzOr22a^{WT(D201A)}$,
867 $DsuzOr22a^{(A201)}$, and wild-type *D. melanogaster* ab3A neurons to a panel of ten
868 odorants, each tested at a 10^{-4} dilution. One-way ANOVA followed by Tukey's multiple
869 comparison test; n = 10. Values indicated with different letters are significantly different.
870 Error bars represent SEM.
871

872 (D) Responses of wild-type *D. suzukii* ab3A neurons, *DsuzOr22a*$^{WT(D201A)}$,
873 *DsuzOr22a*$^{(A201)}$, and wild-type *D. melanogaster* ab3A neurons to different dilutions of
874 isobutyl acetate. One-way ANOVA followed by Tukey's multiple comparison test; n = 10.
875 Values indicated with different letters are significantly different. Error bars represent
876 SEM.
877
878 **Figure 5. Responses of *D. suzukii Or67a* paralogs to a battery of 119 odorants.**
879 (A) Responses of *Dsuz*-ab10A, *DsuzOr67a1*, *DsuzOr67a2*, and *DsuzOr67a1+2* to a
880 battery of 119 odorants, each tested at a 10-4 dilution. n = 5. Error bars represent SEM.
881
882 (B) Responses of *Dsuz*-ab2B, *DsuzOr67a3*, *DsuzOr67a4*, and *DsuzOr67a3+4* to a
883 battery of 119 odorants, each tested at a 10-4 dilution. n = 5. Error bars represent SEM.
884
885
886 (C) Responses of ab2B neurons in wildtype *D. suzukii*, *DsuzOr67a*$^{1/+}$, *DsuzOr67a*$^{2/+}$,
887 *DsuzOr67a*^{1}, and *DsuzOr67a*^{2} to a panel of 15 odorants, each tested at a 10^{-4} dilution.
888 One-way ANOVA followed by Tukey's multiple comparison test; n = 10. Values
889 indicated with different letters are significantly different. Error bars represent SEM.
890
891 (D) Diagrams of ab2 and ab10 sensilla showing the expression of Or67a paralogs in
892 ab10A and ab2B neurons of *D. suzukii*.
893
894 **Figure 6. Evolution of the Or67a subfamily in *D. biarmipes*.**
895 (a) Maximum-likelihood protein tree inferred for *D. biarmipes* Or67a paralogs, *D. suzukii*
896 Or67a paralogs, and *D. melanogaster* Or67a. Node values indicate bootstrap support
897 based on 1,000 replicates. The scale bar represents the number of amino acid
898 substitutions per site. Gene structures are depicted with black boxes for exons and
899 yellow lines for introns.
900
901 (b) Responses of *D. biarmipes* ab10A, ab2B, and *Or67a* paralogs to a battery of 119
902 odorants. n = 5. Error bars represent SEM.
903
904 (C) Principal component analysis of the data from Figures 5A, 5B, and 6B. Percentages
905 along the axes indicate the proportion of variance explained by each principal
906 component.
907
908 (D) Model showing how *Or67a* paralogs are expressed in ab10A and ab2B neurons of
909 *D. suzukii*.
910
911 **Supplementary Tables and Figures**
912 **Table 1. List of odorants**

Odorants	**Source**	Catalog number
1-Heptanol	Millipore Sigma	72954
1-Nonanol	Millipore Sigma	74280
1-Octen-3-ol	Millipore Sigma	O5284
1-Propanol	Millipore Sigma	34871

2,3-Butanediol	Millipore Sigma	B84904
2-Methyl-1-butanol	Millipore Sigma	133051
2-Methyl-1-propanol	Millipore Sigma	538132
3-Methyl-1-butanol	Millipore Sigma	77664
2-Phenylethanol	Millipore Sigma	77861
6-Methyl-5-hepten-2-ol	Millipore Sigma	W488401
Ethanol	Millipore Sigma	459828
Farnesol	Millipore Sigma	43348
trans-2-Hexen-1-ol	Millipore Sigma	W256218
Butyraldehyde	Millipore Sigma	538191
Hexanal	Millipore Sigma	18109
Phenylacetaldehyde	Millipore Sigma	W287407
trans-2-Hexen-1-al	Millipore Sigma	132659
trans-2-nonenal	TCI America	N04835ML
trans,trans-2,4-nonadienal	TCI America	N05215ML
2,3-Butanedione	Millipore Sigma	11038
2-Acetoxy-3-butanone	Millipore Sigma	W352623
2-Heptanone	Millipore Sigma	537683
2-Nonanone	Millipore Sigma	W278505
3-Nonanone	Millipore Sigma	
3-Octanone	Millipore Sigma	136913
4-Methyl-3-hepten-2-one	Millipore Sigma	49722
Acetone	Millipore Sigma	90872
Acetophenone	Millipore Sigma	42163
2-Ethylhexanoic acid	Millipore Sigma	538701
2-Methylbutyric acid	Millipore Sigma	193070
2-Oxovaleric acid	Millipore Sigma	75950
3-Butenoic acid	Millipore Sigma	134716
Acetic acid	Millipore Sigma	A6283
Butyric acid	Millipore Sigma	B103500
Heptanoic acid	Millipore Sigma	W334804
Hexanoic acid	Millipore Sigma	153745
Isobutyric acid	Millipore Sigma	W222208
Linoleic acid	Millipore Sigma	62230
Myristic acid	Millipore Sigma	W276413
Octanoic acid	Millipore Sigma	C2875
Oleic acid	Millipore Sigma	O1008
Pentanoic acid	Millipore Sigma	75054
Propionic acid	Millipore Sigma	402907
trans-3-Hexenoic acid	Millipore Sigma	W317004
Benzyl acetate	Millipore Sigma	50475
Benzyl butyrate	Millipore Sigma	W214000
Butyl acetate	Millipore Sigma	W217417
Butyl butyrate	Millipore Sigma	W218618
Butyl hexanoate	Millipore Sigma	W220108

Butyl isovalerate	Millipore Sigma	W221805
cis-3-hexenyl acetate	Millipore Sigma	74597
cis-3-hexenyl butyrate	Millipore Sigma	W340210
cis-3-hexenyl lactate	Millipore Sigma	W369020
Citronellyl acetate	Millipore Sigma	W231118
Diethyl succinate	Millipore Sigma	W237701
Ethyl (methylthio)acetate	Millipore Sigma	W383503
Ethyl 3-(methylthio)propionate	Millipore Sigma	W334308
Ethyl 3-hydroxybutyrate	Thermo Scientific Chemicals	AC118540250
Ethyl 3-hydroxyhexanoate	Millipore Sigma	W354503
Ethyl acetate	Millipore Sigma	L000325ML
Ethyl benzoate	Millipore Sigma	W242217
Ethyl butyrate	Millipore Sigma	75563
Ethyl decanoate	Millipore Sigma	148970
Ethyl Heptanoate	Millipore Sigma	W243728
Ethyl hexanoate	Millipore Sigma	148962
Ethyl isovalerate	Millipore Sigma	71607
Ethyl lactate	TCI America	L000325ML
Ethyl octanoate	Millipore Sigma	W244910
Ethyl salicylate	Millipore Sigma	68291
Ethyl *trans*-2-butenoate	TCI America	C0418
Ethyl *trans*-2-octenoate	Millipore Sigma	W364304
Geranyl acetate	Millipore Sigma	173495
Hexyl-2-methylbutanoate	Millipore Sigma	W349909
Hexyl hexanoate	Millipore Sigma	W257206
Isoamyl acetate	Millipore Sigma	W205532
Isoamyl butyrate	Millipore Sigma	W206008
Isobutyl acetate	Thermo Scientific Chemicals	AAB2570009
Methyl benzoate	Millipore Sigma	18344
Methyl hexanoate	Millipore Sigma	259942
Methyl isobutyrate	Millipore Sigma	W269409
Methyl octanoate	Millipore Sigma	21719
Methyl salicylate	Millipore Sigma	76631
Pentyl acetate	Millipore Sigma	109584
Phenethyl propionate	Millipore Sigma	W286702
Phenyl acetate	Millipore Sigma	108723
trans-2-Hexenyl acetate	Millipore Sigma	W256404
α-Terpinyl acetate	Millipore Sigma	W304799
4-Ethylguaiacol	Millipore Sigma	39774
4-Methyl veratrole	Millipore Sigma	ALNH9A9DBBB4
Guaiacol	Millipore Sigma	W253200
Indole	TCI America	I002125G
p-Cresol	Millipore Sigma	42429
Veratrole	Millipore Sigma	W379905
Eugenol	Millipore Sigma	35995

Methyl Eugenol	Millipore Sigma	04607
1,4-Diaminobutane	Millipore Sigma	D13208
2-Phenylethylamine	Millipore Sigma	8073340005
Ammonia hydroxide	Millipore Sigma	338818
Cadaverine	Millipore Sigma	33211
Spermidine	Millipore Sigma	S2626
Pyridine	Millipore Sigma	27040
Pyrrolidine	Millipore Sigma	W352316
(+)-Limonene oxide	Millipore Sigma	218324
(R)-(+)-Limonene	Millipore Sigma	62118
(S)-(-)-Limonene	Millipore Sigma	62128
(-)-Menthone	Millipore Sigma	63677
(-)-*trans*-Caryophyllene	Millipore Sigma	75541
Farnesene	Millipore Sigma	W383902
Sabinene	Millipore Sigma	W530597
Terpinolene	Millipore Sigma	W304603
Valencene	Millipore Sigma	W344303
α-Ionone	Millipore Sigma	03642
α-Phellandrene	Millipore Sigma	W285611
α-Pinene	Millipore Sigma	147524
α-Terpineol	Millipore Sigma	04899
β-Citronellol	Millipore Sigma	C83201
β-Cyclocitral	Thermo Scientific Chemicals	AAB2570009
β-Ionone	Millipore Sigma	W259525
γ-Terpinene	Millipore Sigma	223190
γ-Decalactone	Millipore Sigma	93738
γ-Hexalactone	Millipore Sigma	68554
1-Heptadecene	Millipore Sigma	H1108
DEET	Millipore Sigma	36542
Diallyl disulfide	Millipore Sigma	30648

913

914 **Table 2. List of primers for UAS constructs**

	Forward primer (5’ to 3’)	**Reverse primer (5’ to 3’)**
DsuzOr22a	ATGTTAGCCAAATTTTTTCCGC	CTATTTAAACTTTTCGGCTAAG
DsuzOr23a-1	ATGAAACTCAGCAAGATTTCCG	TTATTTAAATGAAACTTGAGTTGGATG
DsuzOr23a-2	ATGAAACTCAGCAAGATCTTTG	TTACAAAAAAGAACCTTGGCCATC
DsuzOr23a-3	ATGGAACTCACCAAGATCCTTG	TTAAGTCCTCCGGTTTAGGGAG
DsuzOr23a-4	ATGGAACTCACCAAGATCCATG	TTATTTAAATGAAACTTGAGTTGGATG

DsuzOr23a-1+4	Or23a1 part: ATGAAACTCAGCAAGATTTCCG	Or23a1 part: tgttctttcactgactgagtttttgcagatggctggaaatgaaacttgagctggatggtc
	Or23a4 part: tcagtcagtgaaagaacaaaaccagacaggatggaactcaccaagatccttgagattgac	Or23a4 part: ttaaaatgaaactttagttggatg
DsuzOr67a-1	ATGATTGATTTAATAAAACAAAAAATTTTTG	TTACTTGTACATCATTCGAACGG
DsuzOr67a-2	ATGAGCATTGACTTAAAAAAGAAG	CTACTGATACATCATTCGAATGG
DsuzOr67a-3	ATGGCTATTAACTTGTTTAGAAAGG	TTACTGATACATTGTTCGAATGG
DsuzOr67a-4	ATGAGTGTCCAGTTTATCAAAAAAC	TTATTGACACACTGTTTTTATAGC
DsuzOr67a-5	ATGAGGGTCGACTCCTTGAAG	CTACTGATACATAGTTCGAAGAGC
DbiaOr67a-1	ATGGTTGTTGGCTTTCTAAAG	TTACTTATACATCATTCGAACAG
DbiaOr67a-2	ATGTGGATTAACTTCATAAGG	CTACTGATACATCATTCGAATG
DbiaOr67a-3	ATGGTCATTAAAGTATTTAGGAAG	TTACTGATACATCGTTCGAATG
DbiaOr67a-5	ATGAGTTTCGATTTCTTAAGG	TCACGGATACATAGTGCGAAG
Note: flanking regions were added to the forward (5'-CAACTTAAAAAAAAAAATCAAA-3') and reverse (5'-TAAAAACGATTCATTCTAGA-3') primers.		

Table 3. Primers for CRISPR

	Forward primer (5' to 3')	**Reverse primer (5' to 3')**
DsuzOr22a gRNA synthesize	TAATACGACTCACTATAGcactttcctctgaccaagca	TTCTAGCTCTAAAACtgcttggtcagaggaaagtg
DsuzOr22a screen	tgccaatatcgattgtcgtg	atactgaccgtgggacaaaca
DsuzOr67a4 gRNA synthesize	TAATACGACTCACTATAGATCGATGCCATACGTTGAGT	TTCTAGCTCTAAAACACTCAACGTATGGCATCGAT
DsuzOr67a4 screen	CGAGTCCTCGAAACCTGAAG	ATGCCGAACACCACGTTTAT

Figure S1. Responses of ORNs housed in D. suzukii and *D. melanogaster* antennal Basiconic, and intermediate, and trichoid sensilla.
(A,B) Heatmaps of responses of ORNs housed in *D. suzukii* (A) and *D. melanogaster* (B) antennal basiconic, intermediate, and trichoid sensilla to 113 odorants. Each odorant was diluted in hexane and tested at a 10^{-2} dilution. Odorants are color coded by functional group.

Figure S2. Responses of 117 individual large basiconic sensilla in *DsuzOrco*^{3} to β-cyclocitral.

Figure S3. Generation of *DsuzOr67a4* mutant alleles.
(A,B) Schematics illustrating the generation of *DsuzOr67a4*^{1} (A) *and DsuzOr67a4*^{2} (B) mutants using CRISPR/Cas9-mediated gene disruption. Nucleotides in red represent the PAM site, underlined nucleotides indicate the gRNA sequence, and dashed lines denote deleted nucleotides.

(C) RNA sequencing data for *DsuzOr67a4* and *DsuzOr67a3*. Green boxes represent exons, and green lines represent introns.

References

1 Benton, R. *Drosophila* olfaction: past, present and future. *Proc Biol Sci* **289**, 20222054, doi:10.1098/rspb.2022.2054 (2022).

2 Hansson, B. S. & Stensmyr, M. C. Evolution of insect olfaction. *Neuron* **72**, 698-711, doi:10.1016/j.neuron.2011.11.003 (2011).

3 Joseph, R. M. & Carlson, J. R. *Drosophila* Chemoreceptors: A Molecular Interface Between the Chemical World and the Brain. *Trends Genet* **31**, 683-695, doi:10.1016/j.tig.2015.09.005 (2015).

4 Montell, C. Drosophila sensory receptors-a set of molecular Swiss Army Knives. *Genetics* **217**, 1-34, doi:10.1093/genetics/iyaa011 (2021).

5 Andersson, M. N., Löfstedt, C. & Newcomb, R. D. Insect olfaction and the evolution of receptor tuning. *Frontiers in Ecology and Evolution* **Volume 3 - 2015**, doi:10.3389/fevo.2015.00053 (2015).

6 Auer, T. O., Shahandeh, M. P. & Benton, R. *Drosophila sechellia*: A Genetic Model for Behavioral Evolution and Neuroecology. *Annu Rev Genet* **55**, 527-554, doi:10.1146/annurev-genet-071719-020719 (2021).

7 Keesey, I. W. Sensory neuroecology and multimodal evolution across the genus Drosophila. *Frontiers in Ecology and Evolution* **Volume 10 - 2022**, doi:10.3389/fevo.2022.932344 (2022).

8 Nozawa, M. & Nei, M. Evolutionary dynamics of olfactory receptor genes in *Drosophila* species. *Proc Natl Acad Sci U S A* **104**, 7122-7127, doi:10.1073/pnas.0702133104 (2007).

9 Peláez, J. N. *et al.* Evolution of chemosensory and detoxification gene families across herbivorous Drosophilidae. *G3 Genes|Genomes|Genetics* **13**, doi:10.1093/g3journal/jkad133 (2023).

10 Sánchez-Gracia, A., Vieira, F. G. & Rozas, J. Molecular evolution of the major chemosensory gene families in insects. *Heredity* **103**, 208-216, doi:10.1038/hdy.2009.55 (2009).

11 Eyun, S. I. *et al.* Evolutionary history of chemosensory-related gene families across the Arthropoda. *Mol Biol Evol* **34**, 1838-1862, doi:10.1093/molbev/msx147 (2017).
12 McBride, C. S., Arguello, J. R. & O'Meara, B. C. Five Drosophila genomes reveal nonneutral evolution and the signature of host specialization in the chemoreceptor superfamily. *Genetics* **177**, 1395-1416, doi:10.1534/genetics.107.078683 (2007).
13 Dweck, H. K., Talross, G. J., Wang, W. & Carlson, J. R. Evolutionary shifts in taste coding in the fruit pest *Drosophila suzukii*. *Elife* **10**, doi:10.7554/eLife.64317 (2021).
14 Karageorgi, M. *et al.* Evolution of Multiple Sensory Systems Drives Novel Egg-Laying Behavior in the Fruit Pest *Drosophila suzukii*. *Curr Biol* **27**, 847-853, doi:10.1016/j.cub.2017.01.055 (2017).
15 Yeh, D. A., Drummond, F. A., Gómez, M. I. & Fan, X. The economic impacts and management of spotted wing *Drosophila* (*Drosophila Suzukii*): The case of wild blueberries in Maine. *Journal of Economic Entomology* **113**, 1262-1269, doi:10.1093/jee/toz360 (2020).
16 Auer, T. O., Álvarez-Ocaña, R., Cruchet, S., Benton, R. & Arguello, J. R. Copy number changes in co-expressed odorant receptor genes enable selection for sensory differences in *drosophilid* species. *Nat Ecol Evol* **6**, 1343-1353, doi:10.1038/s41559-022-01830-y (2022).
17 Goldman-Huertas, B. *et al.* Evolution of herbivory in *Drosophilidae* linked to loss of behaviors, antennal responses, odorant receptors, and ancestral diet. *Proc Natl Acad Sci U S A* **112**, 3026-3031, doi:10.1073/pnas.1424656112 (2015).
18 Matsunaga, T. *et al.* Evolution of Olfactory Receptors Tuned to Mustard Oils in Herbivorous Drosophilidae. *Mol Biol Evol* **39**, doi:10.1093/molbev/msab362 (2022).
19 Matsunaga, T. *et al.* Odorant receptors mediating avoidance of toxic mustard oils in *Drosophila melanogaster* are expanded in herbivorous relatives. *bioRxiv*, doi:10.1101/2024.10.08.617316 (2025).
20 Shaw, K. H., Johnson, T. K., Anderson, A., de Bruyne, M. & Warr, C. G. Molecular and Functional Evolution at the Odorant Receptor Or22 Locus in *Drosophila melanogaster*. *Molecular Biology and Evolution* **36**, 919-929, doi:10.1093/molbev/msz018 (2019).
21 Durkin, S. M. *et al.* Behavioral and Genomic Sensory Adaptations Underlying the Pest Activity of *Drosophila suzukii*. *Mol Biol Evol* **38**, 2532-2546, doi:10.1093/molbev/msab048 (2021).
22 Hickner, P. V. *et al.* The making of a pest: Insights from the evolution of chemosensory receptor families in a pestiferous and invasive fly, *Drosophila suzukii*. *BMC Genomics* **17**, 648, doi:10.1186/s12864-016-2983-9 (2016).
23 Ramasamy, S. *et al.* The Evolution of olfactory gene families in *Drosophila* and the genomic basis of chemical-Ecological adaptation in *Drosophila suzukii*. *Genome Biol Evol* **8**, 2297-2311, doi:10.1093/gbe/evw160 (2016).
24 Walker, W. B., 3rd *et al.* Comparative transcriptomic assessment of the chemosensory receptor repertoire of *Drosophila suzukii* adult and larval olfactory organs. *Comp Biochem Physiol Part D Genomics Proteomics* **45**, 101049, doi:10.1016/j.cbd.2022.101049 (2023).
25 Benton, R. *et al.* An integrated anatomical, functional and evolutionary view of the *Drosophila* olfactory system. *EMBO reports* **0**, 1-22, doi:https://doi.org/10.1038/s44319-025-00476-8 (2025).
26 Dweck, H. K. M. *et al.* The Olfactory Logic behind Fruit Odor Preferences in Larval and Adult *Drosophila*. *Cell Rep* **23**, 2524-2531, doi:10.1016/j.celrep.2018.04.085 (2018).
27 Hallem, E. A. & Carlson, J. R. Coding of odors by a receptor repertoire. *Cell* **125**, 143-160, doi:10.1016/j.cell.2006.01.050 (2006).

1010 28 Hickner, P. V. *et al.* The making of a pest: Insights from the evolution of chemosensory
1011 receptor families in a pestiferous and invasive fly, *Drosophila suzukii*. *BMC Genomics* **17**,
1012 648, doi:10.1186/s12864-016-2983-9 (2016).
1013 29 Dweck, H. K. *et al.* Olfactory channels associated with the *Drosophila* maxillary palp
1014 mediate short- and long-range attraction. *Elife* **5**, doi:10.7554/eLife.14925 (2016).
1015 30 Xue, Q., Hasan, K. S., Dweck, O., Ebrahim, S. A. M. & Dweck, H. K. M. Functional
1016 characterization and evolution of olfactory responses in coeloconic sensilla of the global
1017 fruit pest *Drosophila suzukii*. *BMC Biol* **23**, 50, doi:10.1186/s12915-025-02151-9 (2025).
1018 31 Keesey, I. W., Knaden, M. & Hansson, B. S. Olfactory specialization in *Drosophila suzukii*
1019 supports an ecological shift in host preference from rotten to fresh fruit. *J Chem Ecol* **41**,
1020 121-128, doi:10.1007/s10886-015-0544-3 (2015).
1021 32 Keesey, I. W. *et al.* Functional olfactory evolution in *Drosophila* suzukii and the subgenus
1022 Sophophora. *iScience* **25**, 104212, doi:10.1016/j.isci.2022.104212 (2022).
1023 33 Depetris-Chauvin, A. *et al.* Evolution at multiple processing levels underlies odor-guided
1024 behavior in the genus *Drosophila*. *Curr Biol* **33**, 4771-4785 e4777,
1025 doi:10.1016/j.cub.2023.09.039 (2023).
1026 34 Chiu, J. C. *et al.* Genome of Drosophila suzukii, the spotted wing drosophila. *G3 (Bethesda)*
1027 **3**, 2257-2271, doi:10.1534/g3.113.008185 (2013).
1028 35 Ometto, L. *et al.* Linking genomics and ecology to investigate the complex evolution of an
1029 invasive *Drosophila* pest. *Genome Biol Evol* **5**, 745-757, doi:10.1093/gbe/evt034 (2013).
1030 36 Versace, E. *et al.* Physiological and behavioral responses in *Drosophila melanogaster* to
1031 odorants present at different plant maturation stages. *Physiol Behav* **163**, 322-331,
1032 doi:10.1016/j.physbeh.2016.05.027 (2016).
1033 37 Cha, D. H., Adams, T., Rogg, H. & Landolt, P. J. Identification and field evaluation of
1034 fermentation volatiles from wine and vinegar that mediate attraction of spotted wing
1035 *Drosophila, Drosophila suzukii*. *J Chem Ecol* **38**, 1419-1431, doi:10.1007/s10886-012-0196-
1036 5 (2012).
1037 38 Chahda, J. S. *et al.* The molecular and cellular basis of olfactory response to tsetse fly
1038 attractants. *PLoS Genet* **15**, e1008005, doi:10.1371/journal.pgen.1008005 (2019).
1039 39 Shaw, K. H., Johnson, T. K., Anderson, A., de Bruyne, M. & Warr, C. G. Molecular and
1040 Functional Evolution at the Odorant Receptor *Or22* Locus in *Drosophila melanogaster*. *Mol*
1041 *Biol Evol* **36**, 919-929, doi:10.1093/molbev/msz018 (2019).
1042 40 Butterwick, J. A. *et al.* Cryo-EM structure of the insect olfactory receptor Orco. *Nature* **560**,
1043 447-452, doi:10.1038/s41586-018-0420-8 (2018).
1044 41 Crava, C. M., Sassù, F., Tait, G., Becher, P. G. & Anfora, G. Functional transcriptome
1045 analyses of *Drosophila suzukii* antennae reveal mating-dependent olfaction plasticity in
1046 females. *Insect Biochem Mol Biol* **105**, 51-59, doi:10.1016/j.ibmb.2018.12.012 (2019).
1047 42 Dweck, H. K. M. & Carlson, J. R. Molecular Logic and Evolution of Bitter Taste in *Drosophila*.
1048 *Curr Biol* **30**, 17-30.e13, doi:10.1016/j.cub.2019.11.005 (2020).
1049 43 Dekker, T., Ibba, I., Siju, K. P., Stensmyr, M. C. & Hansson, B. S. Olfactory shifts parallel
1050 superspecialism for toxic fruit in *Drosophila melanogaster* sibling, *D. sechellia*. *Curr Biol*
1051 **16**, 101-109, doi:10.1016/j.cub.2005.11.075 (2006).
1052 44 Stensmyr, M. C., Dekker, T. & Hansson, B. S. Evolution of the olfactory code in the
1053 *Drosophila melanogaster* subgroup. *Proc Biol Sci* **270**, 2333-2340,
1054 doi:10.1098/rspb.2003.2512 (2003).
1055 45 Auer, T. O. *et al.* Olfactory receptor and circuit evolution promote host specialization.
1056 *Nature* **579**, 402-408, doi:10.1038/s41586-020-2073-7 (2020).

46 Shaw, K. H. *et al.* Natural variation at the *Drosophila melanogaster Or22* odorant receptor locus is associated with changes in olfactory behaviour. *Open Biol* **11**, 210158, doi:10.1098/rsob.210158 (2021).
47 Mansourian, S. *et al.* Wild African *Drosophila melanogaster* Are Seasonal Specialists on Marula Fruit. *Curr Biol* **28**, 3960-3968 e3963, doi:10.1016/j.cub.2018.10.033 (2018).
48 Crowley-Gall, A. *et al.* Olfactory variation among closely related cactophilic *Drosophila* species. *J Comp Physiol A Neuroethol Sens Neural Behav Physiol*, doi:10.1007/s00359-025-01744-7 (2025).
49 de Bruyne, M., Smart, R., Zammit, E. & Warr, C. G. Functional and molecular evolution of olfactory neurons and receptors for aliphatic esters across the *Drosophila* genus. *J Comp Physiol A Neuroethol Sens Neural Behav Physiol* **196**, 97-109, doi:10.1007/s00359-009-0496-6 (2010).
50 Jumper, J. *et al.* Highly accurate protein structure prediction with AlphaFold. *Nature* **596**, 583-589, doi:10.1038/s41586-021-03819-2 (2021).
51 O'Boyle, N. M. *et al.* Open Babel: An open chemical toolbox. *J Cheminform* **3**, 33, doi:10.1186/1758-2946-3-33 (2011).

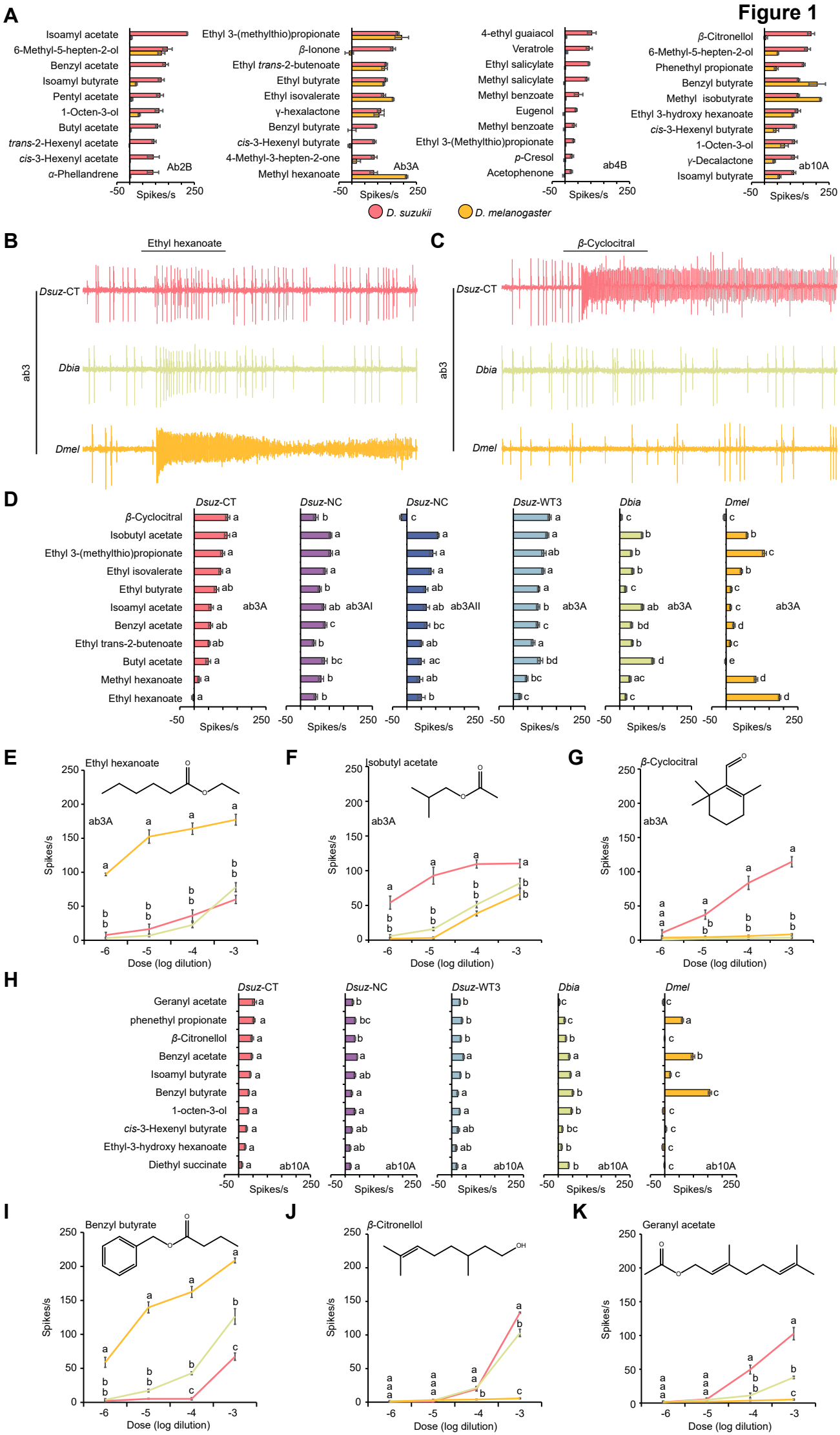
Figure 1
A
Isoamyl acetate
6-Methyl-5-hepten-2-ol
Benzyl acetate
Isoamyl butyrate
Pentyl acetate
1-Octen-3-ol
Butyl acetate
trans-2-Hexenyl acetate
cis-3-Hexenyl acetate
α-Phellandrene
Ab2B
Ethyl 3-(methylthio)propionate
β-Ionone
Ethyl trans-2-butenoate
Ethyl butyrate
Ethyl isovalerate
γ-hexalactone
Benzyl butyrate
cis-3-Hexenyl butyrate
4-Methyl-3-hepten-2-one
Methyl hexanoate
Ab3A
4-ethyl guaiacol
Veratrole
Ethyl salicylate
Methyl salicylate
Methyl benzoate
Eugenol
Methyl benzoate
Ethyl 3-(Methylthio)propionate
p-Cresol
Acetophenone
ab4B
β-Citronellol
6-Methyl-5-hepten-2-ol
Phenethyl propionate
Benzyl butyrate
Methyl isobutyrate
Ethyl 3-hydroxy hexanoate
cis-3-Hexenyl butyrate
1-Octen-3-ol
γ-Decalactone
Isoamyl butyrate
ab10A
-50
Spikes/s
250
D. suzukii
D. melanogaster
B
Ethyl hexanoate
Dsuz-CT
Dbia
Dmel
ab3
C
β-Cyclocitral
D
Dsuz-CT
Dsuz-NC
Dsuz-NC
Dsuz-WT3
Dbia
Dmel
β-Cyclocitral
Isobutyl acetate
Ethyl 3-(methylthio)propionate
Ethyl isovalerate
Ethyl butyrate
Isoamyl acetate
Benzyl acetate
Ethyl trans-2-butenoate
Butyl acetate
Methyl hexanoate
Ethyl hexanoate
ab3A
ab3AI
ab3AII
ab3A
ab3A
ab3A
E
Ethyl hexanoate
ab3A
Spikes/s
Dose (log dilution)
F
Isobutyl acetate
ab3A
G
β-Cyclocitral
ab3A
H
Dsuz-CT
Dsuz-NC
Dsuz-WT3
Dbia
Dmel
Geranyl acetate
phenethyl propionate
β-Citronellol
Benzyl acetate
Isoamyl butyrate
Benzyl butyrate
1-octen-3-ol
cis-3-Hexenyl butyrate
Ethyl-3-hydroxy hexanoate
Diethyl succinate
ab10A
I
Benzyl butyrate
J
β-Citronellol
K
Geranyl acetate

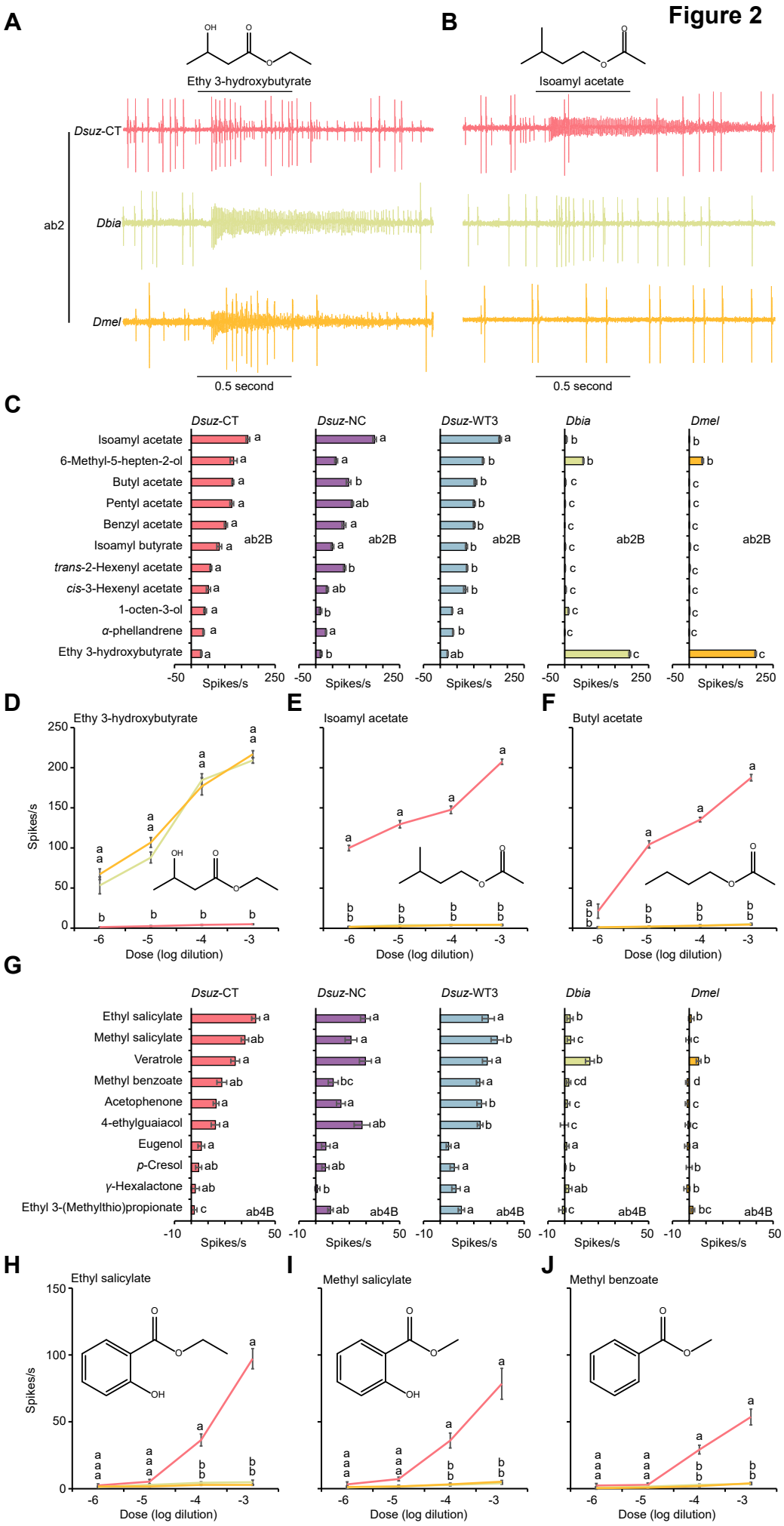
Figure 2
A
B
Ethy 3-hydroxybutyrate
Isoamyl acetate
Dsuz-CT
Dbia
Dmel
ab2
0.5 second
C
Dsuz-CT
Dsuz-NC
Dsuz-WT3
Dbia
Dmel
Isoamyl acetate
6-Methyl-5-hepten-2-ol
Butyl acetate
Pentyl acetate
Benzyl acetate
Isoamyl butyrate
trans-2-Hexenyl acetate
cis-3-Hexenyl acetate
1-octen-3-ol
α-phellandrene
Ethy 3-hydroxybutyrate
ab2B
Spikes/s
D
E
F
Ethy 3-hydroxybutyrate
Isoamyl acetate
Butyl acetate
Spikes/s
Dose (log dilution)
G
Ethyl salicylate
Methyl salicylate
Veratrole
Methyl benzoate
Acetophenone
4-ethylguaiacol
Eugenol
p-Cresol
γ-Hexalactone
Ethyl 3-(Methylthio)propionate
ab4B
Spikes/s
H
I
J
Ethyl salicylate
Methyl salicylate
Methyl benzoate
Spikes/s
Dose (log dilution)

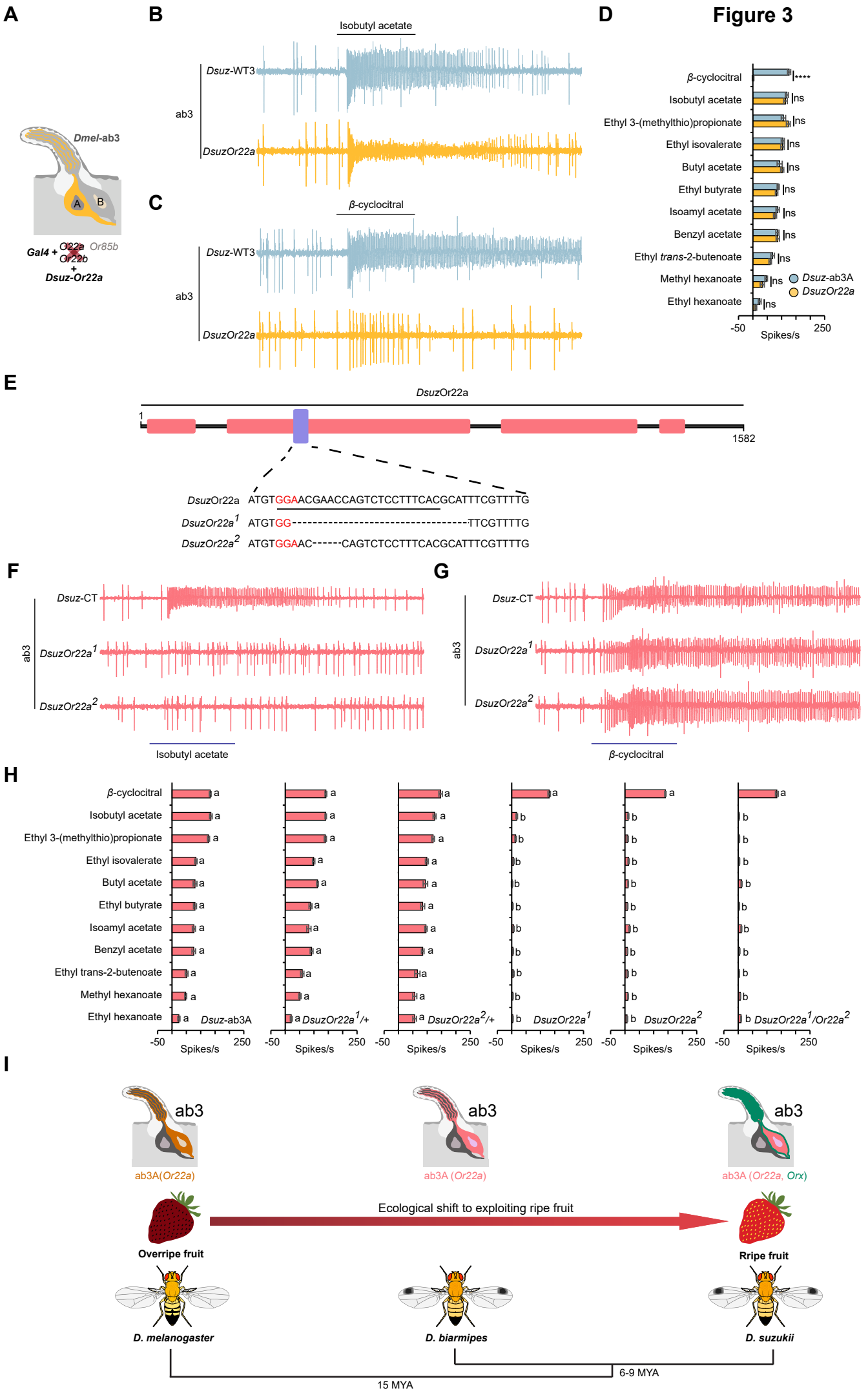
Figure 3
A
Dmel-ab3
A
B
Gal4 + Or22a Or85b
Or22b
+
Dsuz-Or22a
B
Isobutyl acetate
ab3
Dsuz-WT3
DsuzOr22a
C
β-cyclocitral
ab3
Dsuz-WT3
DsuzOr22a
D
β-cyclocitral
Isobutyl acetate
Ethyl 3-(methylthio)propionate
Ethyl isovalerate
Butyl acetate
Ethyl butyrate
Isoamyl acetate
Benzyl acetate
Ethyl trans-2-butenoate
Methyl hexanoate
Ethyl hexanoate
****
ns
Dsuz-ab3A
DsuzOr22a
-50
Spikes/s
250
E
DsuzOr22a
1
1582
DsuzOr22a ATGTGGAACGAACCAGTCTCCTTTCACGCATTTCGTTTTG
DsuzOr22a1 ATGTGG----------TTCGTTTTG
DsuzOr22a2 ATGTGGAAC------CAGTCTCCTTTCACGCATTTCGTTTTG
F
ab3
Dsuz-CT
DsuzOr22a1
DsuzOr22a2
Isobutyl acetate
G
ab3
Dsuz-CT
DsuzOr22a1
DsuzOr22a2
β-cyclocitral
H
β-cyclocitral
Isobutyl acetate
Ethyl 3-(methylthio)propionate
Ethyl isovalerate
Butyl acetate
Ethyl butyrate
Isoamyl acetate
Benzyl acetate
Ethyl trans-2-butenoate
Methyl hexanoate
Ethyl hexanoate
Dsuz-ab3A
DsuzOr22a1/+
DsuzOr22a2/+
DsuzOr22a1
DsuzOr22a2
DsuzOr22a1/Or22a2
a
b
-50
Spikes/s
250
I
ab3
ab3A(Or22a)
ab3
ab3A (Or22a)
ab3
ab3A (Or22a, Orx)
Ecological shift to exploiting ripe fruit
Overripe fruit
Rripe fruit
D. melanogaster
D. biarmipes
D. suzukii
15 MYA
6-9 MYA

Figure 4

A

```
                pid
DmelOr22a       100.0%  MLSKFFPHIKEKPLSERVKSRDAFIYLDRVMWSFGWTEPENKRWILPYKLWLAFVNIVML  60
DsuzOr22a       69.8%   MLAKFFPLIKERPLNERVQSRDAFIYLDRVMWTLGWTEPYEKRWAAVYKVFCFLTTMVCF  60
DbiaOr22a       69.0%   MLIKFFPLIKEKPLNELVQSRDAFIYLERVMWTLGWTEPYEKRWAVVYKVFSFMTSIGFF  60
                                                                          TM1
DmelOr22a       100.0%  ILLPISISIEYLHRFKTFSAGEFLSSLEIGVNMYGSSFKCAFTLIGFKKRQEAKVLLDQL  120
DsuzOr22a       69.8%   ILVPISIVVEYVRRFKSFSAGEFLSSLEIGVNMYGCSFKNTYTLLGQRKVRKAKLILDRL  120
DbiaOr22a       69.0%   ILLPLSICVEYVNRFKSFSAGEFLSSLEIGVNMCGCSFKNTYTLLGRRKVRKAKLILDRL  120
                                          TM2
DmelOr22a       100.0%  DKRCLSDKERSTVHRYVAMGNFFDILYHIFYSTFVVMNFPYFLLERRHAWRMYFPYIDSD  180
DsuzOr22a       69.8%   DERCLRDEEKSLVHRYVALGNFSYVVYHTCYWVFVITNFIGFLLIGHHAWRMFIPLLKSD  180
DbiaOr22a       69.0%   DERCLRDEEKSLVHRYVALGNFSYTVYHTCYWVFVITNFIGFLLIGHHAWRMYIPLLKSD  180
                                          TM3
DmelOr22a       100.0%  EQFYISSIAECFLMTEAIYMDLCTDVCPLISMLMARCHISLLKQRLRNLRSKPGRTEDEY  240
DsuzOr22a       69.8%   EHFLISSVAEFLLMLYVVTMAQCSDVCPTVSMLMARCHILLLQKRVLRLRSDPGKGDDED  240
DbiaOr22a       69.0%   EHFLISSVAEFLLMLYVVTMAQCSDVCPTISMLMARCHIILLRNRMMRLRSDPEKGDDED  240
                             TM4
DmelOr22a       100.0%  LEELTECIRDHRLLLDYVDALRPVFSGTIFVQFLLIGTVLGLSMINLMFFSTFWTGVATC  300
DsuzOr22a       69.8%   LEELAKCIQDHHLILDYVNTLRPVFSGVIFVQFLLIGVVLGLSMINVMFFLSFWTGLGTC  300
DbiaOr22a       69.0%   LEELTKCIQDHRLILDYVNTLRPVFSGVIFVQFLLIGVVLGLSMINVMFFLSFWTGLGTC  300
                                          TM5                                TM6
DmelOr22a       100.0%  LFMFDVSMETFPFCYLCNMIIDDCQEMSNCLFQSDWTSADRRYKSTLVYFLHNLQQPITL  360
DsuzOr22a       69.8%   LFMFDVCMETFPFCYLCNMIIDDCQDLSDSLFQSNWTSASRRYKSTLVYFLHNLQQPIIL  360
DbiaOr22a       69.0%   LFMFDVCMETFPFCYLCNIIIDDCQDLADSLFQSNWTSASRRYKSTLVYFLHNLQQPIIL  360
                                                                   TM7
DmelOr22a       100.0%  TAGGVFPISMQTNLAMVKLAFSVVTVIKQFNLAERFQ  397
DsuzOr22a       69.8%   TAGGVFPICMQTNLSMVKLAFSVVTIIKQFNLAEKFK  397
DbiaOr22a       69.0%   TAGGIFPICMQTNLSMVKLAFSVVTIIKQFNLADKFK  397
```

B

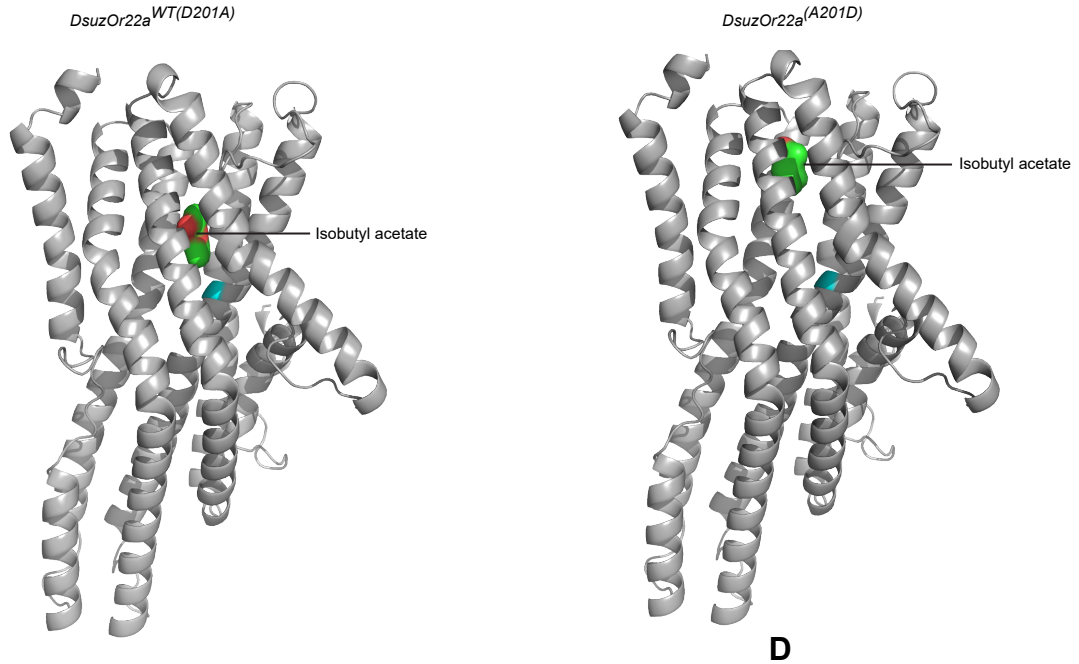

C

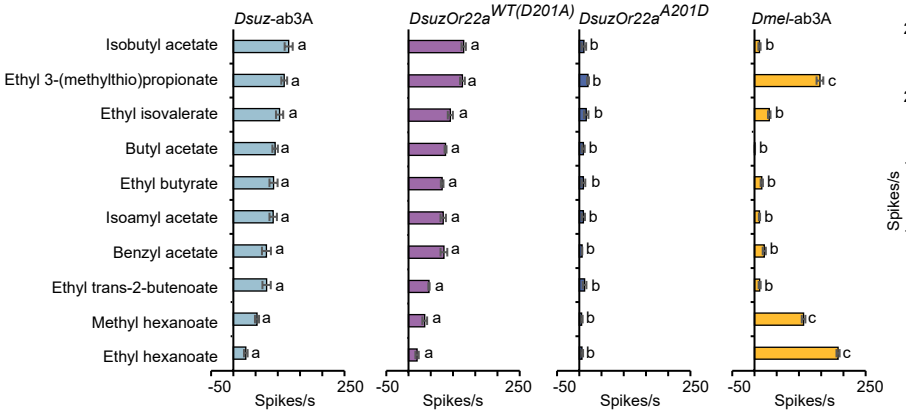

D

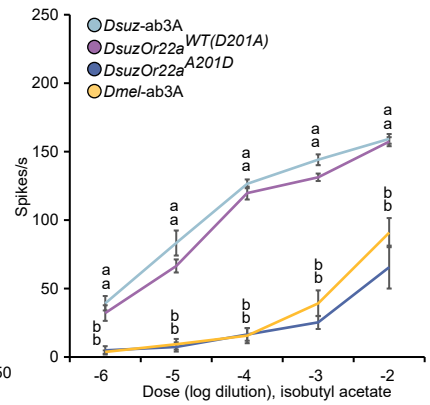

Figure 5

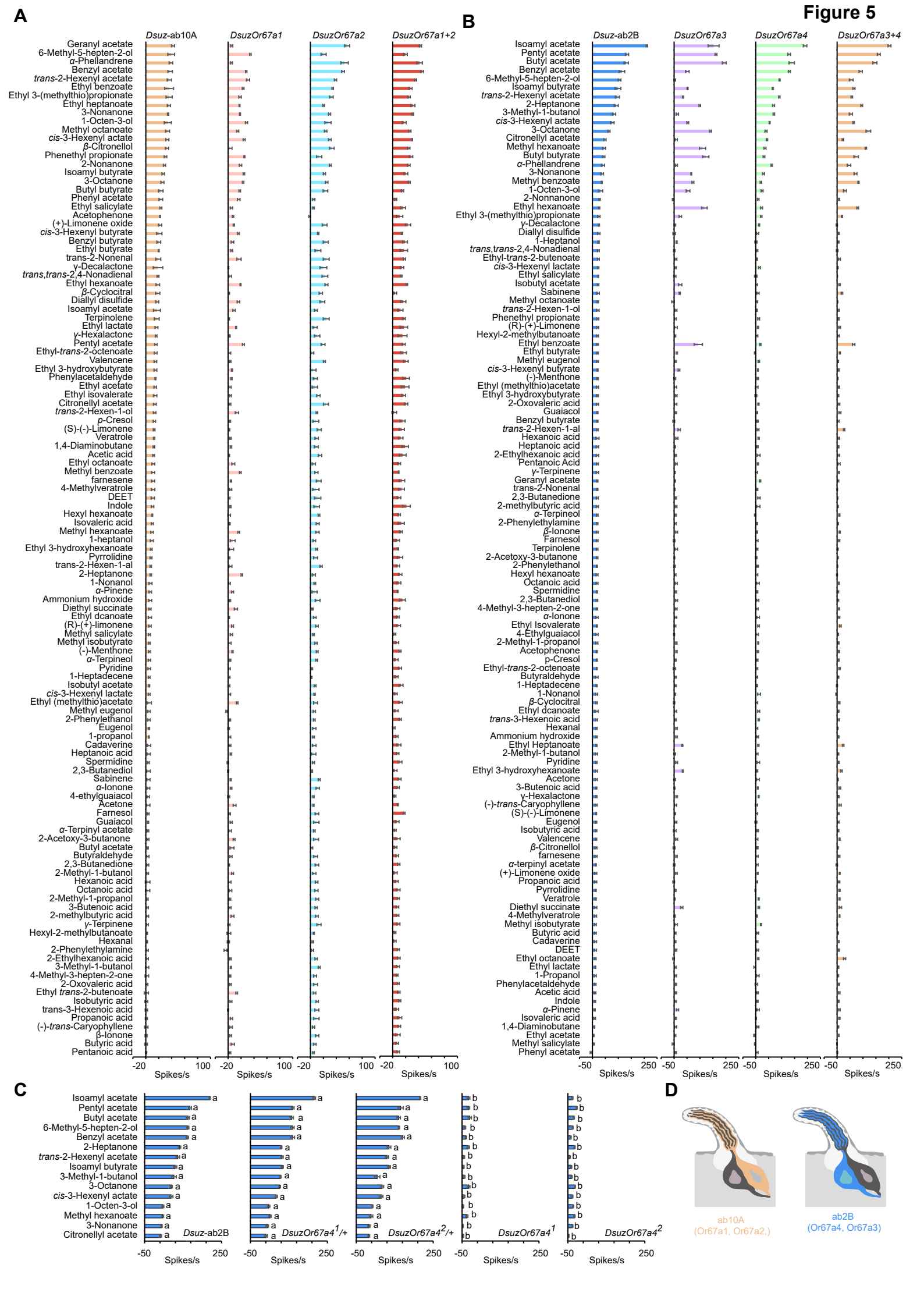
A
Dsuz-ab10A
DsuzOr67a1
DsuzOr67a2
DsuzOr67a1+2
Geranyl acetate
6-Methyl-5-hepten-2-ol
α-Phellandrene
Benzyl acetate
trans-2-Hexenyl acetate
Ethyl benzoate
Ethyl 3-(methylthio)propionate
Ethyl heptanoate
3-Nonanone
1-Octen-3-ol
Methyl octanoate
cis-3-Hexenyl actate
β-Citronellol
Phenethyl propionate
2-Nonanone
Isoamyl butyrate
3-Octanone
Butyl butyrate
Phenyl acetate
Ethyl salicylate
Acetophenone
(+)-Limonene oxide
cis-3-Hexenyl butyrate
Benzyl butyrate
Ethyl butyrate
trans-2-Nonenal
γ-Decalactone
trans,trans-2,4-Nonadienal
Ethyl hexanoate
β-Cyclocitral
Diallyl disulfide
Isoamyl acetate
Terpinolene
Ethyl lactate
γ-Hexalactone
Pentyl acetate
Ethyl-trans-2-octenoate
Valencene
Ethyl 3-hydroxybutyrate
Phenylacetaldehyde
Ethyl acetate
Ethyl isovalerate
Citronellyl acetate
trans-2-Hexen-1-ol
p-Cresol
(S)-(-)-Limonene
Veratrole
1,4-Diaminobutane
Acetic acid
Ethyl octanoate
Methyl benzoate
farnesene
4-Methylveratrole
DEET
Indole
Hexyl hexanoate
Isovaleric acid
Methyl hexanoate
1-heptanol
Ethyl 3-hydroxyhexanoate
Pyrrolidine
trans-2-Hexen-1-al
2-Heptanone
1-Nonanol
α-Pinene
Ammonium hydroxide
Diethyl succinate
Ethyl dcanoate
(R)-(+)-limonene
Methyl salicylate
Methyl isobutyrate
(-)-Menthone
α-Terpineol
Pyridine
1-Heptadecene
Isobutyl acetate
cis-3-Hexenyl lactate
Ethyl (methylthio)acetate
Methyl eugenol
2-Phenylethanol
Eugenol
1-propanol
Cadaverine
Heptanoic acid
Spermidine
2,3-Butanediol
Sabinene
α-Ionone
4-ethylguaiacol
Acetone
Farnesol
Guaiacol
α-Terpinyl acetate
2-Acetoxy-3-butanone
Butyl acetate
Butyraldehyde
2,3-Butanedione
2-Methyl-1-butanol
Hexanoic acid
Octanoic acid
2-Methyl-1-propanol
3-Butenoic acid
2-methylbutyric acid
γ-Terpinene
Hexyl-2-methylbutanoate
Hexanal
2-Phenylethylamine
2-Ethylhexanoic acid
3-Methyl-1-butanol
4-Methyl-3-hepten-2-one
2-Oxovaleric acid
Ethyl trans-2-butenoate
Isobutyric acid
trans-3-Hexenoic acid
Propanoic acid
(-)-trans-Caryophyllene
β-Ionone
Butyric acid
Pentanoic acid
-20
100
Spikes/s
B
Dsuz-ab2B
DsuzOr67a3
DsuzOr67a4
DsuzOr67a3+4
Isoamyl acetate
Pentyl acetate
Butyl acetate
Benzyl acetate
6-Methyl-5-hepten-2-ol
Isoamyl butyrate
trans-2-Hexenyl acetate
2-Heptanone
3-Methyl-1-butanol
cis-3-Hexenyl actate
3-Octanone
Citronellyl acetate
Methyl hexanoate
Butyl butyrate
α-Phellandrene
3-Nonanone
Methyl benzoate
1-Octen-3-ol
2-Nonnanone
Ethyl hexanoate
Ethyl 3-(methylthio)propionate
γ-Decalactone
Diallyl disulfide
1-Heptanol
trans,trans-2,4-Nonadienal
Ethyl-trans-2-butenoate
cis-3-Hexenyl lactate
Ethyl salicylate
Isobutyl acetate
Sabinene
Methyl octanoate
trans-2-Hexen-1-ol
Phenethyl propionate
(R)-(+)-Limonene
Hexyl-2-methylbutanoate
Ethyl benzoate
Ethyl butyrate
Methyl eugenol
cis-3-Hexenyl butyrate
(-)-Menthone
Ethyl (methylthio)acetate
Ethyl 3-hydroxybutyrate
2-Oxovaleric acid
Guaiacol
Benzyl butyrate
trans-2-Hexen-1-al
Hexanoic acid
Heptanoic acid
2-Ethylhexanoic acid
Pentanoic Acid
γ-Terpinene
Geranyl acetate
trans-2-Nonenal
2,3-Butanedione
2-methylbutyric acid
α-Terpineol
2-Phenylethylamine
β-Ionone
Farnesol
Terpinolene
2-Acetoxy-3-butanone
2-Phenylethanol
Hexyl hexanoate
Octanoic acid
Spermidine
2,3-Butanediol
4-Methyl-3-hepten-2-one
α-Ionone
Ethyl Isovalerate
4-Ethylguaiacol
2-Methyl-1-propanol
Acetophenone
p-Cresol
Ethyl-trans-2-octenoate
Butyraldehyde
1-Heptadecene
1-Nonanol
β-Cyclocitral
Ethyl dcanoate
trans-3-Hexenoic acid
Hexanal
Ammonium hydroxide
Ethyl Heptanoate
2-Methyl-1-butanol
Pyridine
Ethyl 3-hydroxyhexanoate
Acetone
3-Butenoic acid
γ-Hexalactone
(-)-trans-Caryophyllene
(S)-(-)-Limonene
Eugenol
Isobutyric acid
Valencene
β-Citronellol
farnesene
α-terpinyl acetate
(+)-Limonene oxide
Propanoic acid
Pyrrolidine
Veratrole
Diethyl succinate
4-Methylveratrole
Methyl isobutyrate
Butyric acid
Cadaverine
DEET
Ethyl octanoate
Ethyl lactate
1-Propanol
Phenylacetaldehyde
Acetic acid
Indole
α-Pinene
Isovaleric acid
1,4-Diaminobutane
Ethyl acetate
Methyl salicylate
Phenyl acetate
-50
250
Spikes/s
C
Isoamyl acetate
Pentyl acetate
Butyl acetate
6-Methyl-5-hepten-2-ol
Benzyl acetate
2-Heptanone
trans-2-Hexenyl acetate
Isoamyl butyrate
3-Methyl-1-butanol
3-Octanone
cis-3-Hexenyl actate
1-Octen-3-ol
Methyl hexanoate
3-Nonanone
Citronellyl acetate
Dsuz-ab2B
DsuzOr67a4 1/+
DsuzOr67a4 2/+
DsuzOr67a4 1
DsuzOr67a4 2
a
b
-50
250
Spikes/s
D
ab10A
(Or67a1, Or67a2,)
ab2B
(Or67a4, Or67a3)

Figure 6

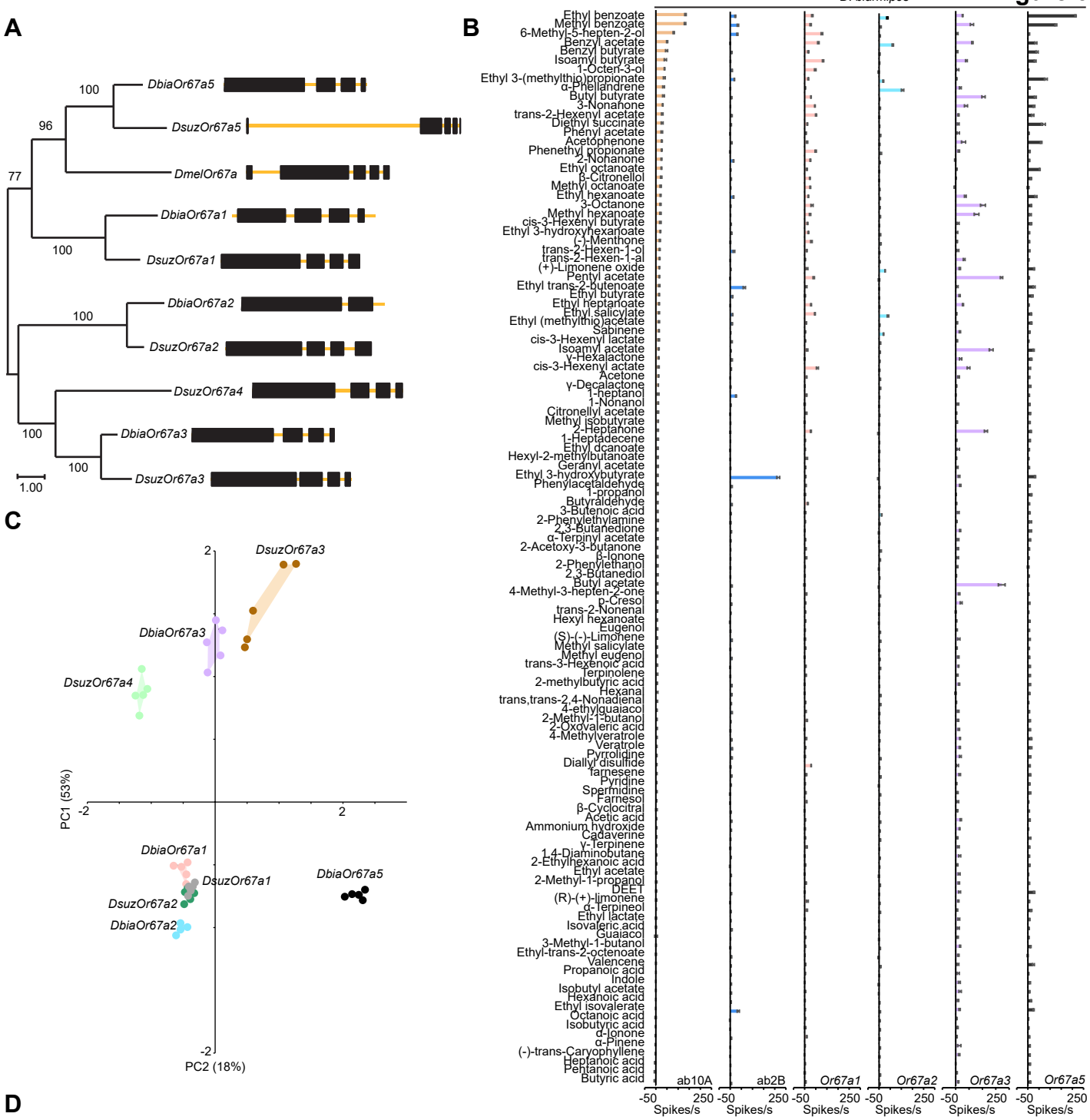

D

Model showing how *Or67a* paralogs are expressed in ab10A and ab2B neurons of *D. suzukii*.

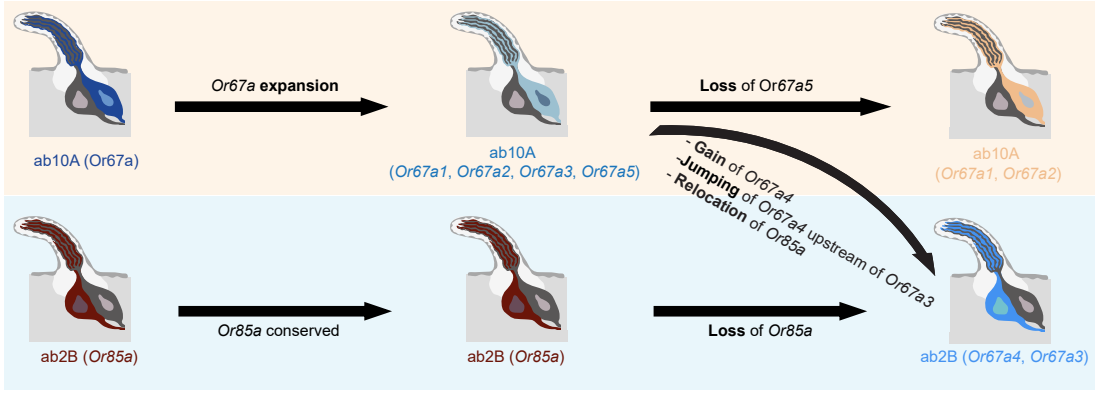

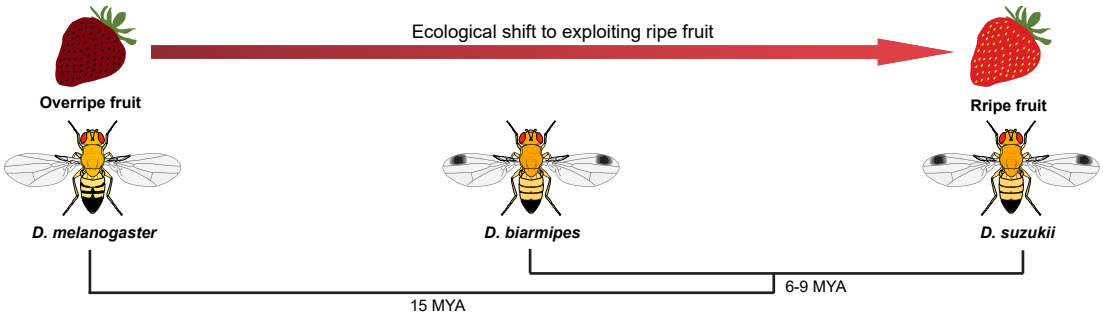

Figure S1

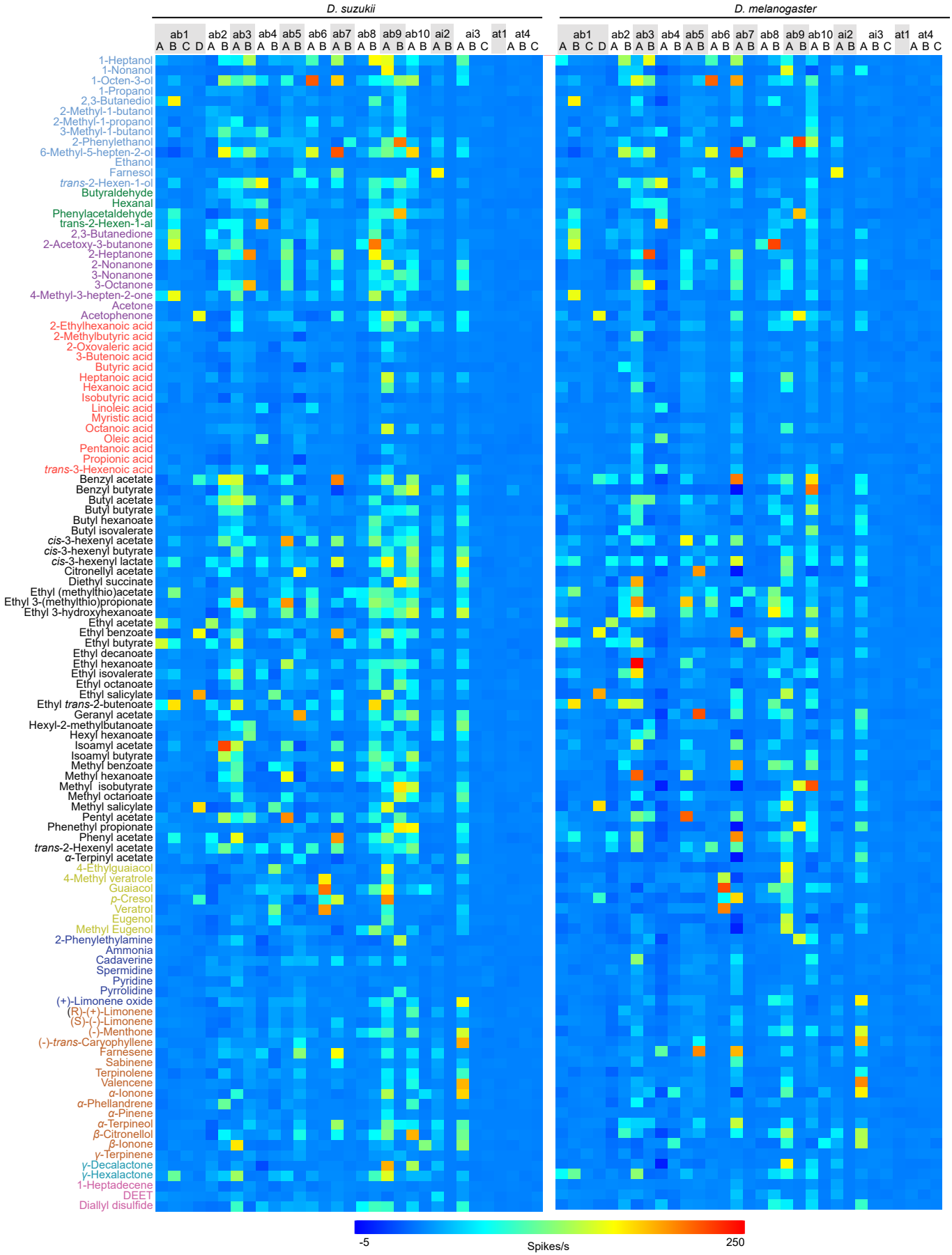
D. suzukii
D. melanogaster
ab1 A B C D
ab2 A B
ab3 A B
ab4 A B
ab5 A B
ab6 A B
ab7 A B
ab8 A B
ab9 A B
ab10 A B
ai2 A B
ai3 A B C
at1
at4 A B C
1-Heptanol
1-Nonanol
1-Octen-3-ol
1-Propanol
2,3-Butanediol
2-Methyl-1-butanol
2-Methyl-1-propanol
3-Methyl-1-butanol
2-Phenylethanol
6-Methyl-5-hepten-2-ol
Ethanol
Farnesol
trans-2-Hexen-1-ol
Butyraldehyde
Hexanal
Phenylacetaldehyde
trans-2-Hexen-1-al
2,3-Butanedione
2-Acetoxy-3-butanone
2-Heptanone
2-Nonanone
3-Nonanone
3-Octanone
4-Methyl-3-hepten-2-one
Acetone
Acetophenone
2-Ethylhexanoic acid
2-Methylbutyric acid
2-Oxovaleric acid
3-Butenoic acid
Butyric acid
Heptanoic acid
Hexanoic acid
Isobutyric acid
Linoleic acid
Myristic acid
Octanoic acid
Oleic acid
Pentanoic acid
Propionic acid
trans-3-Hexenoic acid
Benzyl acetate
Benzyl butyrate
Butyl acetate
Butyl butyrate
Butyl hexanoate
Butyl isovalerate
cis-3-hexenyl acetate
cis-3-hexenyl butyrate
cis-3-hexenyl lactate
Citronellyl acetate
Diethyl succinate
Ethyl (methylthio)acetate
Ethyl 3-(methylthio)propionate
Ethyl 3-hydroxyhexanoate
Ethyl acetate
Ethyl benzoate
Ethyl butyrate
Ethyl decanoate
Ethyl hexanoate
Ethyl isovalerate
Ethyl octanoate
Ethyl salicylate
Ethyl trans-2-butenoate
Geranyl acetate
Hexyl-2-methylbutanoate
Hexyl hexanoate
Isoamyl acetate
Isoamyl butyrate
Methyl benzoate
Methyl hexanoate
Methyl isobutyrate
Methyl octanoate
Methyl salicylate
Pentyl acetate
Phenethyl propionate
Phenyl acetate
trans-2-Hexenyl acetate
α-Terpinyl acetate
4-Ethylguaiacol
4-Methyl veratrole
Guaiacol
p-Cresol
Veratrol
Eugenol
Methyl Eugenol
2-Phenylethylamine
Ammonia
Cadaverine
Spermidine
Pyridine
Pyrrolidine
(+)-Limonene oxide
(R)-(+)-Limonene
(S)-(-)-Limonene
(-)-Menthone
(-)-trans-Caryophyllene
Farnesene
Sabinene
Terpinolene
Valencene
α-Ionone
α-Phellandrene
α-Pinene
α-Terpineol
β-Citronellol
β-Ionone
γ-Terpinene
γ-Decalactone
γ-Hexalactone
1-Heptadecene
DEET
Diallyl disulfide
-5
Spikes/s
250

Figure S2

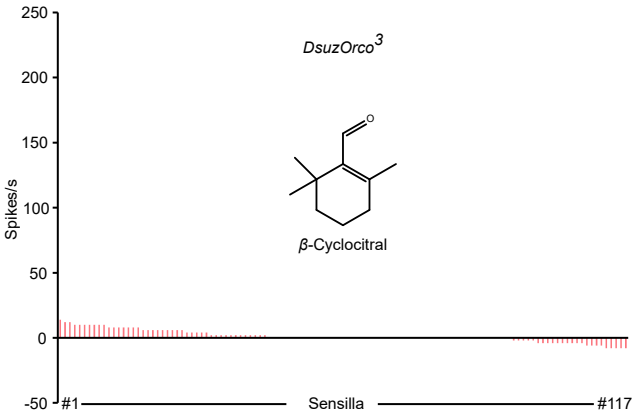
250
200
150
100
50
0
-50
Spikes/s
DsuzOrco3
O
β-Cyclocitral
#1
Sensilla
#117

Figure S3

A

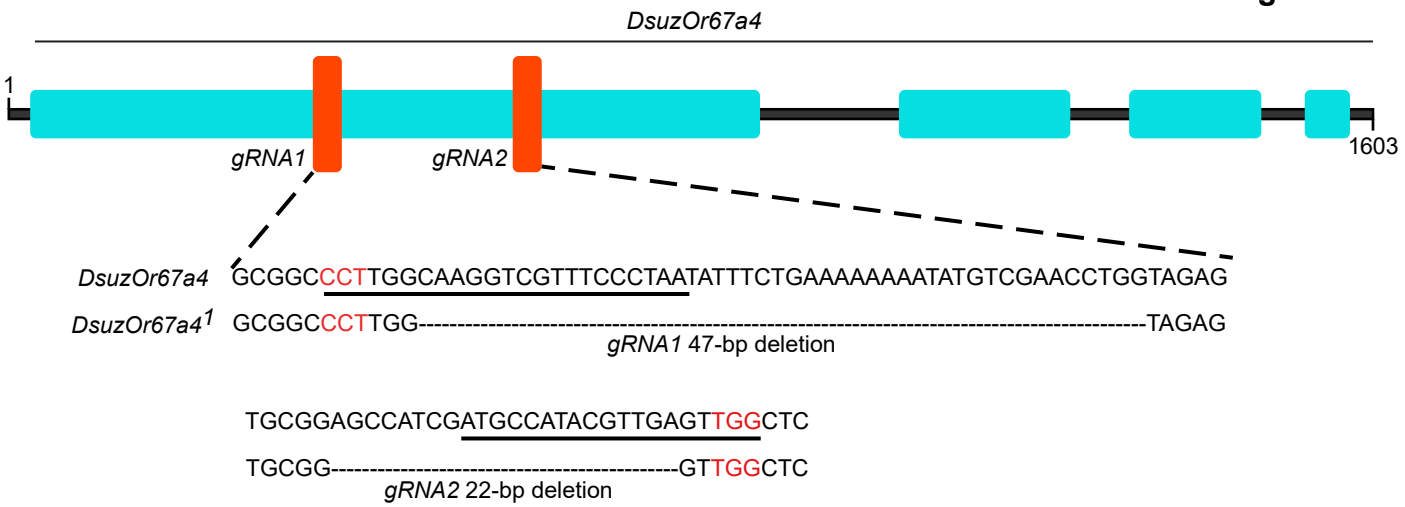

B

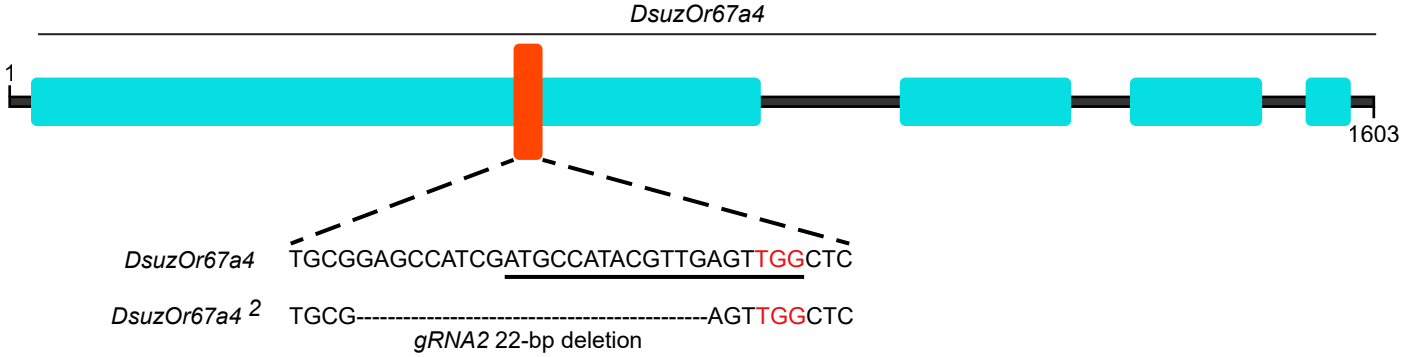
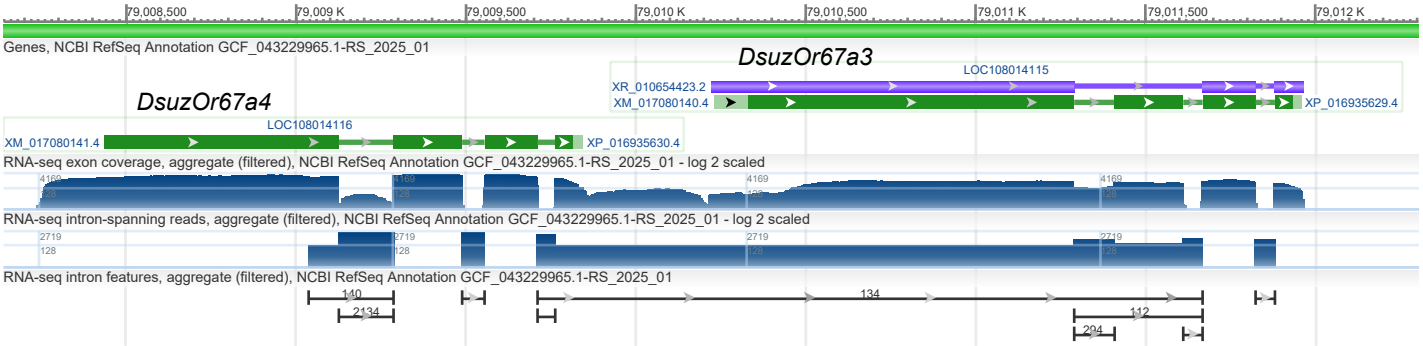
C